Energy Pumping Mechanism for Hopping Robot

M. Tech Dissertation

Submitted in partial fulfillment of the requirements

for the degree of

Master of Technology

By

Vitthal Narayan Londhe

(Roll No. 05310006)

Under the Guidance of

Prof. B. Seth

Department of Mechanical Engineering,

Indian Institute of Technology, Bombay.

(July 2007)

Abstract

For steady state hopping, energy must be imparted in a hopper as there are losses due to impact and friction. This can be achieved with the help of suitable actuator and energy pumping mechanism. In this thesis, several mechanisms are considered for pumping energy in the flight phase of hopping and one such system is designed and fabricated. The same system is also modeled in ADAMS software. The experimental set-up is for a vertical hopper in which energy is pumped by pre-charging the main leg spring with the help of a DC motor and the energy is retained in the spring by the use of a latch mechanism that releases the energy once the hopper hits the ground. Steady state hopping experiments are carried out. Experimental results are compared with results from ADAMS simulation package for the same hopper parameters. It is seen that by tuning the friction parameter in ADAMS simulation, good match is obtained for hopping with different energy injection.

Keywords: Hopping Robot, Steady State Hopping, Energy Pumping, Energy Losses.

CONTENTS

LIST OF TABLES

LIST OF FIGURES

NOMENCLATURE

Δ = Vertical displacement of sensing rod *(m)*

ϕ = Pawl angular displacement *(deg)*

F = Static load on spring *(N)*

d = Spring wire diameter *(m)*

D = Spring mean coil diameter *(m)*

C= Spring index

τ = Shear stress *(N/m^2)*

K_s = Shear stress correction factor *(N/m^2)*

k = Spring rate (stiffness) *(N/m)*

G = Modulus of rigidity *(N/m^2)*

N = Number of active turns of spring coil

F_{max}= Maximum load *(N)*

F_{min} = Minimum load *(N)*

F_a = Amplitude load *(N)*

F_m = Mean load *(N)*

τ_a = Amplitude shear stress *(N/m^2)*

τ_m = Mean shear stress *(N/m^2)*

K_B = Bergstrasser factor

S_{ut} = Ultimate tensile strength *(N/m^2)*

N_e = End coils

N_t =Total number of coils

L_0 = Free length *(m)*

Ls = Solid length *(m)*

p = Coil pitch *(m)*

D_0 = Outer diameter *(m)*

L_0 = Inner diameter *(m)*

τ_{all} = Allowable shear stress *(N/m^2)*

M = Mass of body parts *(kg)*

m = Un-sprung mass *(kg)*

Δh = Change in body position in Y direction from apex point to touch-down *(m)*

V_1 = Velocity of body and leg at touch down *(m/s)*

E_{f1} = Energy loss in guide friction from apex point to touch-down *(J)*

E_1 = Energy loss in impact between leg and ground at touch-down *(J)*

E_{f2} = Energy loss in guide friction from touch-down to mid-stance *(J)*

δ = Spring compression needs for steady state hopping. *(m)*

x = Spring compression from touch-down to mid-stance *(m)*

E_{f3} = Energy loss in guide friction from mid-stance to take-off *(J)*

V_2 = Velocity of body just before take-off *(m/s)*

V_3 = Velocity of body and leg just after take-off *(m/s)*

E_2 = Energy loss in impact between leg and body at take-off *(N-m)*

E_{f4} = Energy loss in guide friction from take-off to apex point (*N-m)*

T_l = Torque on load shaft (*N-m)*

T_m = Torque at motor shaft (*N-m)*

G = Gear reduction ratio

n = Number of revolutions

N_l = Speed of load shaft *(rpm)*

N_m = Speed of motor shaft *(rpm)*

T_c = Motor continuous torque rating *(N-m)*

T_p = Motor peak torque rating *(N-m)*

$N_{m,\,max}$= Maximum speed of motor *(rpm)*

T_{RMS}= Root-mean square value of the required motor torque *(N-m)*

$T_{f,}$ = Time for motor forward rotation *(s)*

T = Total time for motor one oscillation *(s)*

A= Amplitude of angular displacement *(m)*

t = Instantaneous time *(s)*

μ_s = Coefficient of static friction

μ_d = Coefficient of dynamic friction

ABBREVIATIONS

PE - Potential Energy

KE – Kinetic Energy

SLOM- Springy Leg Offset Mass

COM- Center of Mass

SLIP- Spring Leg Inverted Pendulum

LM- Linear Motion

DOF- Degree of Freedom

DC- Direct Current

PWM- Pulse Width Modulation

LED – Light Emitting Diode

NC - Normally Closed

NO - Normally Open

PID – Proportional, Integral and Derivative

Chapter 1

INTRODUCTION

1.1 Motivation:

Legged robots and legged locomotion are now an area of intense research, as the limitations of wheeled or tracked vehicles are obvious when it comes to locomotion on rough terrain. The study of legged locomotion is also important to understand the human and animal walking, as well as, running behavior and to build machines that have mobility on rough terrain and artificial leg for amputees.

A legged machine needs much more complex coordination and control as compared wheeled vehicle. In this regard, single legged machines offer simplified approach to understand the complexity of locomotion. As the number of legs increase in a walking machine, the coordination of legs complicates the dynamics and control of the system. On the other hand, single legged machines, not only have no leg coordination problem but also work with a minimum level of actuations and reduced weight as compared with multi legged machines. Also, due to the springiness of legs used for single legged machines, it is possible to utilize part of the body kinetic energy from one hopping cycle to the next. Though multi-legged machines are statically stable (except biped) and therefore easier to control but they generally operate at much lower speed as compared to single legged machines.

1.1.1 Hopper and Energy Pumping:

A single legged robot is the simplest dynamically stablizable machine. The only possible gait for such robots is by hopping. Hopping consists of cyclic combination of stance and flight phase. In flight phase, robot is detached from ground and in stance phase, it can be considered to be attached to the ground. These two phases are separated by events known as touch-down and take-off. In hopping, dimension of obstruction cleared by robot is independent on the leg physical parameters but solely depends on the amount of energy stored in the leg before the takeoff.

A hopping cycle is subjected to energy loss per hop which mainly includes impact losses at touch-down and take-off. At the time of touch-down, inelastic impact of leg on ground results in loss of whole kinetic energy of leg and at take off point, impact occurs between body and leg and losses part of kinetic energy of body. Apart from this in telescopic leg, sliding motion between leg and body in stance phase results in some additional energy loss to overcome friction.

A steady state hopping is possible by maintaining hopper energy at predefined level. So to compensate the losses per hop, hopper needs an external agency like actuator. It pumps some form of energy in each hopping cycle. Energy pumping instant and form of energy are depends on kind of hopper design and actuation technique. Amount of energy pumping is depends on geometry of terrain. On even terrain, hoppers motion results in steady state hopping. In steady state hopping some predefined amount of energy is pumped in each cycle. For uneven terrain, hopper motion results in transient hopping. In transient hopping, energy pump varies for each hopping cycle and it is function of terrain geometry.

1.2 Scope of the Thesis:

The present works aims at the development and testing of energy pumping mechanism for vertical hopper. It includes design and development of efficient and effective energy pumping mechanism which is capable to impart the range of energy in the flight phase. After conceptual development of mechanism, it is simulated in ADAMS to study it for various parameters. To test this mechanism experimentally, a low weight vertical hopper is designed and fabricated. A DC motor is used as external agency to pump the energy. Experimental work includes study of steady state hopping and friction modeling of guide by using ADAMS. Experimental results are compared with ADAMS simulation result for same hopping height.

1.3 Layout of Report:

The report is organized as follows. Chapter 2 comprises of the literature review carried on energy analysis and energy pumping of the hopper. Chapter 3 describes the conceptual development of energy pumping mechanisms and selection of the most suitable mechanism. Chapter 4 includes design consideration and detailed design of experimental set up of the hopper model. Consideration of actuator selection from hopper energy analysis is also included in this chapter. Chapter 5 describes control systems and controller design for the hopper model. Experimental results and ADAMS simulation results are compared in chapter 6. Lastly chapter 7 summarizes the conclusion and future scope.

Chapter 2

LITERATURE REVIEW

2.1 Raibert's Model:

Raibert [1, 2] has done pioneering work in the field of hopping robots. He developed a monopod to study the dynamic stability and energy requirement of single legged machines. His planner hopper is primarily developed to study problems in active balance in dynamics and legged locomotion in a way that could be generalized for multi-legged machines.

2.1.1 Design and Construction:

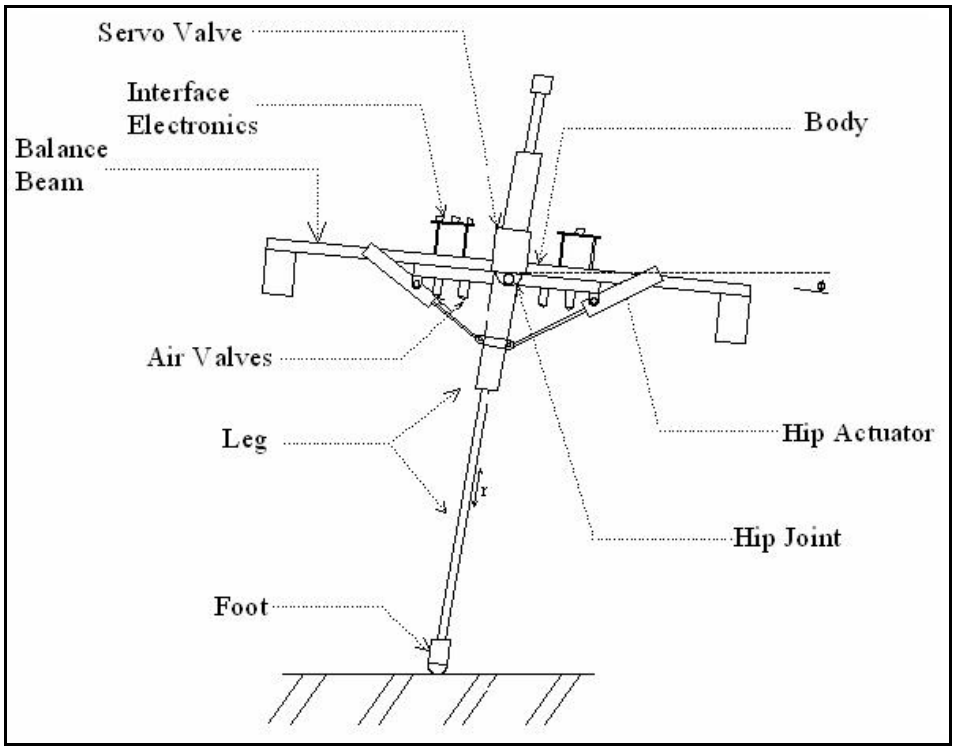

Fig 2.1: Raibert's Planner Hopper [1]

It consists of springy leg and body, connected by hinge type hip. Body consists of platform that carries sensors, actuators, valves and computer interface electronics. The

behavior of hopper was simplified by using tether mechanism (not shown) restricting it's motion to single plane. The tether mechanism constraints to move with just three degrees of freedom; vertical translational, rotation of body about hip joint and forward translational.

The hopper had two actuators: a rotary hip- actuator and a leg spring actuator. The hip actuator consists of a proportional pneumatic pressure-control valve which drove a pair of air cylinders which in turn exerted torques about the hip. The leg consists of a pneumatic cylinder acts as an actuator. The leg moved as a springy inverted pendulum while on the ground. The stiffness of the spring could be controlled by varying the air pressure inside the pneumatic cylinder. It uses four solenoid valves, which connects each chamber of leg cylinder either to atmospheric air through regulated orifice or supply pressure of 90 psi for each cylinder.

2.1.2 Operation of the Machine:

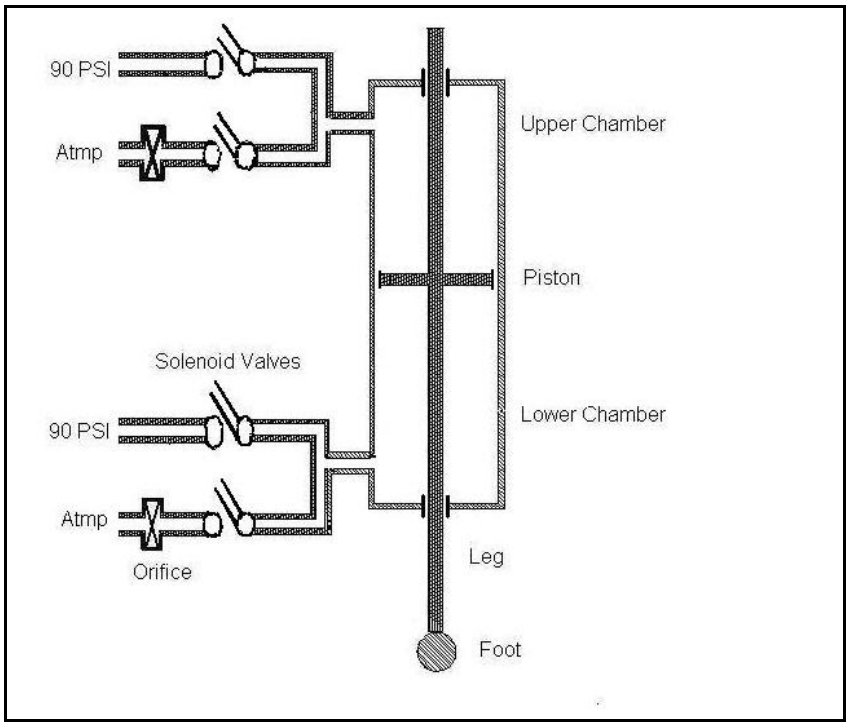

Fig 2.2: Raibert Leg with Pneumatic Actuator [1]

To initiate hopping, the machine is dropped from a shallow height onto the extended leg. Then the control system operates the solenoid valves of the pneumatic air cylinders to excite and sustain hopping motion. The control system applies thrust by opening the supply solenoid valve to the upper chamber of the leg cylinder during each stance. Once the foot leaves the ground, the control system exhausts the upper chamber of the leg cylinder until it reaches designated pressure. Typically it hops at 1.5-3 hops per second and peak to peak body oscillation can be varied 0.04 to 0.3 m.

2.2 Spring Loaded Inverted Pendulum Model (SLIP):-

SLIP model has been extensively used as a simplified model in analysis and control of running legged robots; it considers point-mass body with a springy leg to capture the approximate running dynamics. It has been implemented in a robot and validated experimentally by Akihiro [4, 5].

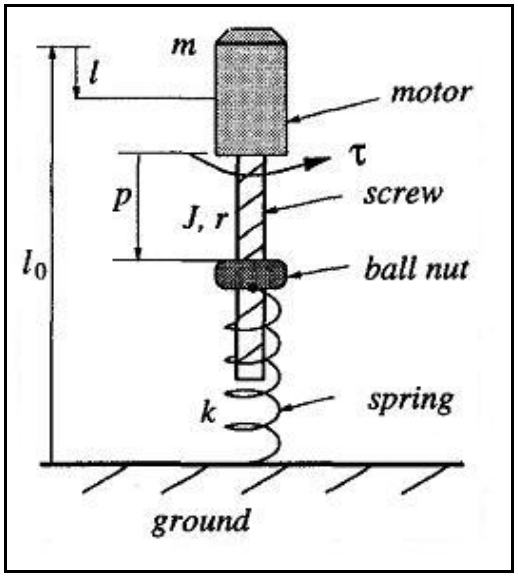

Fig 2.3: SLIP Model [4]

2.2.1 Design and Construction:

Fig 2.3 shows the basic components of SLIP model. It consists of the electrical actuator which is connected to power screw. One end of spring is connected to foot (not shown in Fig 2.3) and other end is connected to the nut, so spring will expand naturally after mid-stance. Ball nut has provided only vertical motion so that when screw rotates, it results in the movement of one end of spring.

2.2.2 Operation of the Machine:

Initially model is dropped from small height. As soon as it touches the ground spring get compressed due to conversion of body potential energy. At the same time, motor starts and additionally compresses the spring. As flight phase begins motor will rotate in opposite direction by same angle as that of angle turned in stance phase and cycle repeats.

2.3 Bow Leg Hopper:

Zeglin [6] has developed new type hopper with flexible leg. Fig 2.4 shows the laboratory set up of bow leg hopper. The Bow Leg hopper has a nonlinear curved laminated fiberglass sheet spring, instead of a linear spring in the SLIP model. Its COM is located below the hip to allow the body to be self-righting while the SLIP model has its COM located in the hip joint

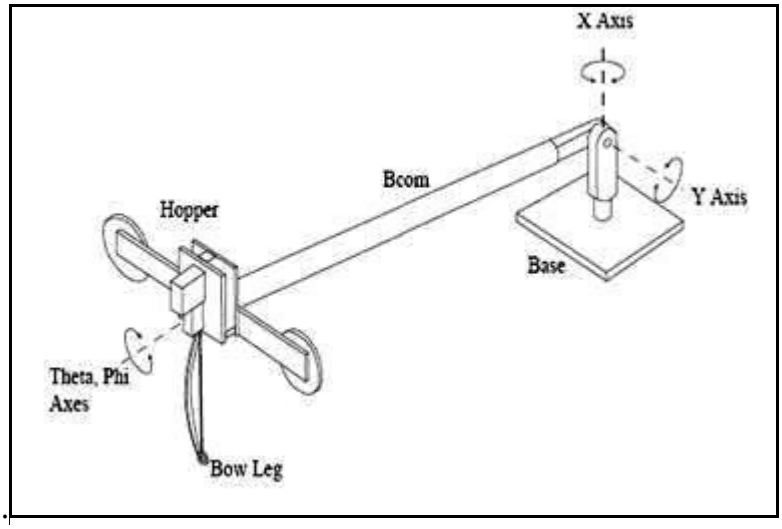

Fig 2.4: Laboratory set up of Bow Leg Hopper [6]

2.3.1 Design and Construction:

Fig 2.5 shows details of bow leg hopper .The bow leg comprises of a curved leaf spring, foot, freely pivoting hip and the bow strings that holds the leg in compression. The string is used to control the potential energy of spring. The leg is positioned using servo motor coupled to foot with control string. It consists of two actuators: leg angle servo and thrust servo.

2.3.2 Operation of Machine:

As flight phase starts, thrust servo rotates disk carrying the pulley (shown in Fig 2.5) that can engage the bow string so as to compress the leg spring to store the energy. After impact string goes slack and string release spring pushes the string off the pulley. The winding direction and string displacement alternates left-right. At the same time leg servo positions the leg. Fig 2.6 shows the detail phases of bow string from relaxed to unwinding.

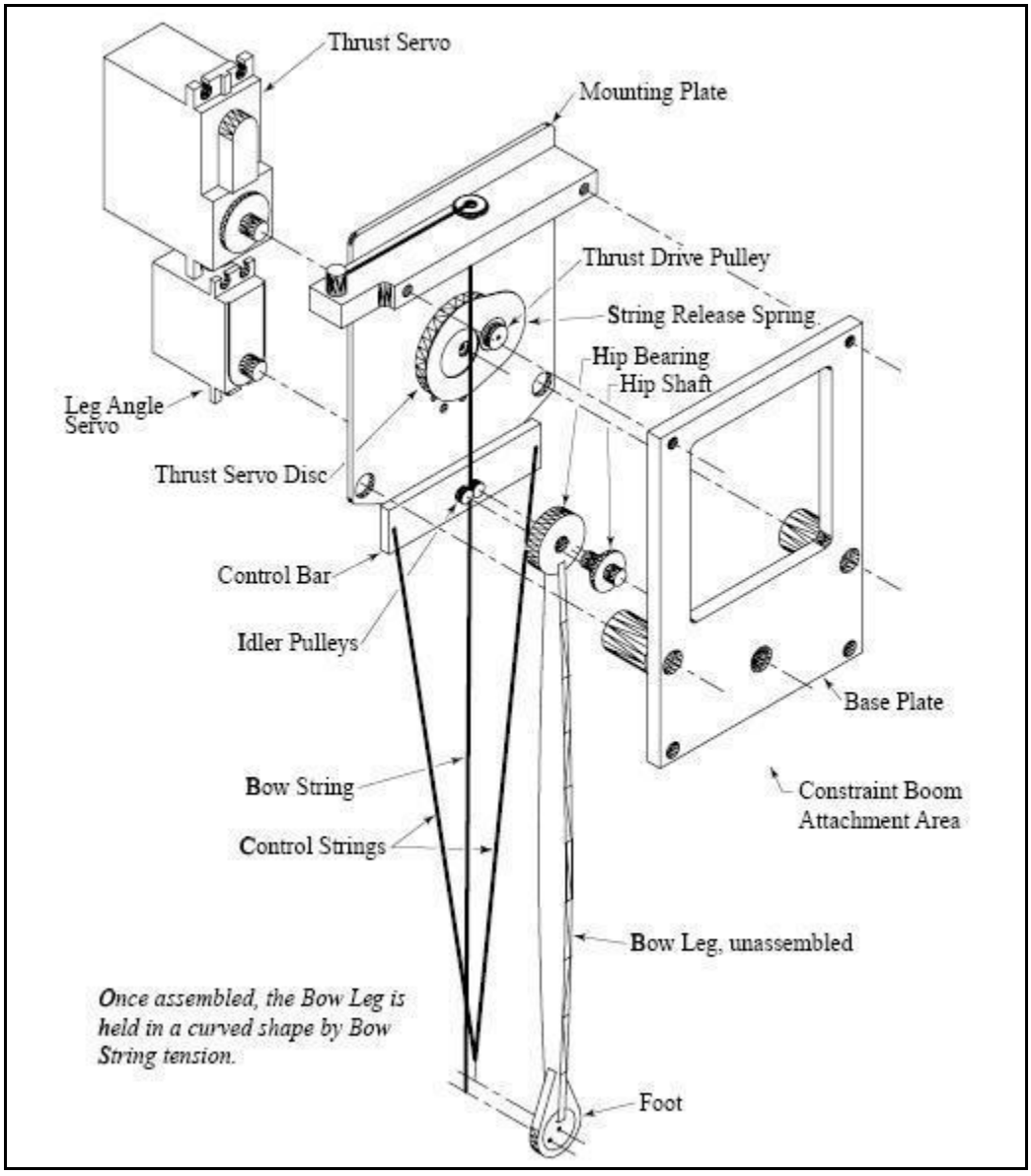

Fig 2.5: Exploded view of the Bow Leg Hopper [6]

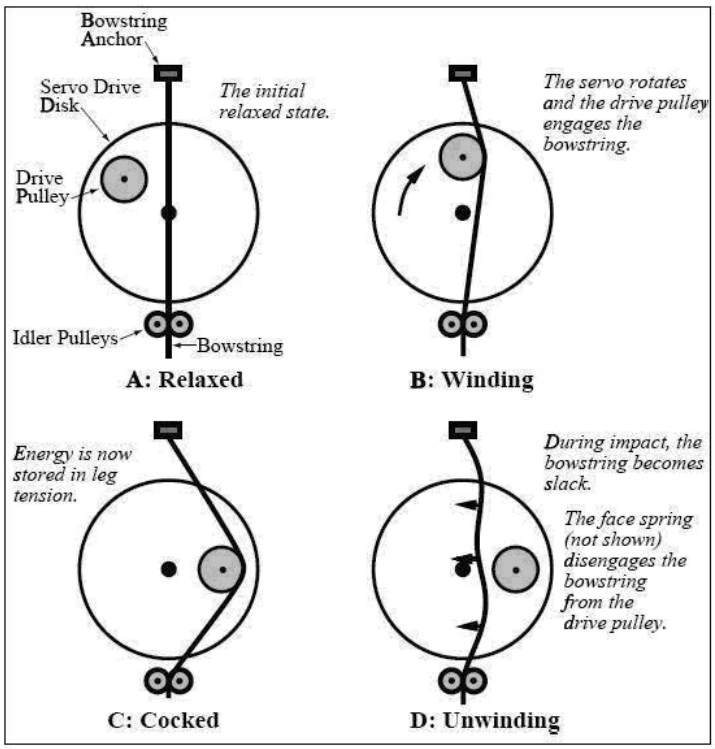

Fig 2.6 Phases of Hopperthrust mechanism [6]

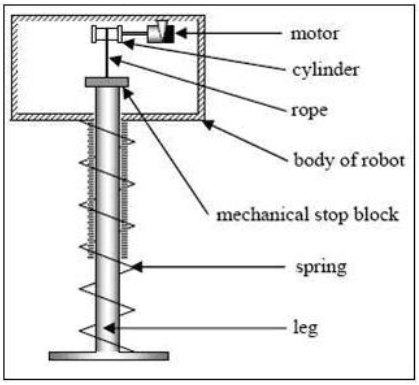

Fig 2.7 Vertical Hopper Model [7]

2.4 Vertical Hopper for Energy Analysis:

Akinfiev *et. al.* [7] made detailed energy analysis of hopping robot. A kinematic configuration of hopper is as shown in Fig 2.9. It consists on telescopic leg, spring, electric actuator, flexible rope, cylinder and body. At the beginning of the flight phage motor turns the cylinder, thus compresses the spring with the help of rope and holds it up to touchdown. After impact, rope slacks and motor rotates in opposite direction equally. As compression spring losses stability and contact with guide rails in deformed state. To reduce the internal losses of energy during the loading and unloading of spring, they replace the compression spring by tension spring of same effective stiffness.

2.5 Springy Leg Offset Mass Hopper (SLOM):

Shanmuganathan [8] analyzes the passive dynamics of SLOM hopping, and observes that the eccentric springy-leg provides self-stabilization of the angular motion, resulting in an extended passive hopping motion. He explored the effect of some under-actuation strategies that use only a single rotary actuator for stabilization of the forward-hopping

motion. Sharma [9] considered SLOM design of hopper with a springy leg and an offset mass. Gebretsadik [10] had modified Sharma's [9] design to reduce weight of hopper and maintains proper alignment between leg and body. Due to the offset mass, the line of action of spring force is not through the centre of gravity of the hopper and an angular velocity is imparted at take-off. This has been found to be helpful in self stabilization, making it possible to achieve passive hopping motion.

2.5.1 Design and Construction:

Fig 2.9 shows SLOM hopper model developed by Sharma [9]. It consists of body and telescopic leg connected to foot by hinge joint. Hopper uses 2 actuators; one for energy compensation to get sustained hopping and other for re-orient the offset mass to get passive hopping.

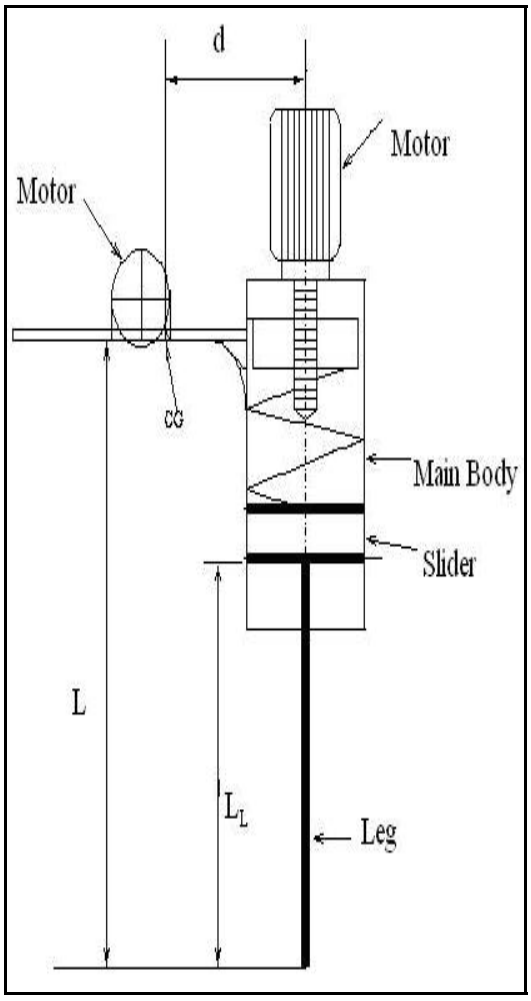

Fig 2.8: SLOM Model [9]

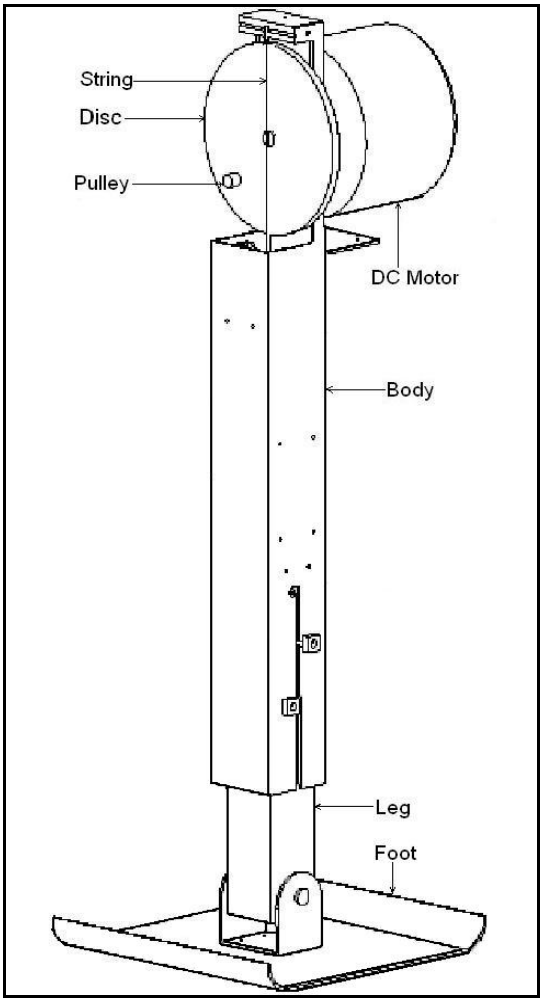

Fig 2.9: SLOM Prototype [9]

To compensate the energy losses in hopping, he uses similar mechanism as that of Zeglin [6], one end of string is connected to top of body and other is connected to leg. A disc with small pulley is mounted on the motor shaft as shown is Fig 2.8.

2.5.2 Operation of Machine:

Here hopper is dropped from small height with small initial pre-compression of spring. In flight phase, it orients the body with help of offset mass and also compresses spring. It holds the spring up to touchdown, string gets release from pulley. Now spring freely releases its energy and results in take-off.

2.6 Actuation Techniques:

Hamidreza [11] reports that powerful hydraulic actuators are harnessed for control of the legged robot. He focuses on a planar one legged hopper, which is electrically actuated. This actuation technology is clean, safe and cheap, suitable for autonomous robots. However, DC motors have much smaller torque to mass ratio than hydraulic actuators, only special consideration must be paid to the modeling, design and control of the hopper.

2.7 Summary from Literature Review:

Many researchers have studied hopper model with different energy actuation techniques like pneumatic, electric etc. They have also used different kind of mechanisms to pump this energy. The main drawback in Zeglin [6] and Sharma [9] mechanisms is actuator must hold the leg at that position up to touch down. Therefore actuator needs some extra power which is not directly useful in hopping.

This power can be saved by using some kind of latching arrangement. The arrangement should unlatch automatically at touch-down.

Chapter 3

DEVELOPMENT OF MECHANISM

The review of different hopping robot uses resonance condition for its motion. It uses spring mass system with telescopic leg. In order to overcome energy losses during hopping cycle, researchers had developed mechanisms with different actuation technique. In electrical actuation, leg must be hold at the given position up to stance phase. This power of holding the leg at that position is not useful for hopping. To overcome this power loss and to reduce the actuator effort, hopper is incorporated with effective energy pumping mechanism. Here, mechanism has to pump the energy in flight time. As flight time is much larger than stance time. If time available to pump the energy is more then low power actuator will fulfill the functional requirements.

3.1 Functional Requirements:

Mechanism should have following functional requirements

1. It should latch the leg at various positions with respect to body, when it has given some pre-defined displacement in one direction and gets locked in other direction.
2. It should automatically unlatch the leg at touch-down point, so that at take-off whole spring energy is released in the form of body kinetic energy.
3. It should capable to pump wide range of energy effectively and efficiently in the flight phase.

3.2 Feasible Mechanisms:

In order to fulfill above functional requirements, mechanism should have latching element like pawl and ratchet. Fig 3.1 shows three feasible mechanisms opted for hopper energy pumping. Each mechanism differs than other mechanism, in latching or kind of effort application.

3.2.1 Mechanism 1:

First mechanism consists of a disc with pulley, a string, a sensing rod, a bell crank mechanism, 2 pawls and ratchets. One end of string is connected is upper end of body and other end is connected to leg through a compression spring (not shown in Fig 3.1). A disc with small pulley is mounted on the actuator shaft. Sensing rod is provided to unlatch the pawl at touch-down, and immediately latches the pawl at take-off.

In flight phase, as motor rotates string get engaged in pulley and get stretched. Stretching of string will result in compression of spring. At desired point of compression, motor stops and immediately returns to its original position. But the pawl and ratchet holds the leg at that position up to the touch-down. At touch-down, sensing rod unlatches the ratchet through bell crank mechanism and releases the whole spring PE into body KE. At take-off, pawl gets engaged in ratchet due to weight of sensing rod. Again next flight phase start and cycle repeats.

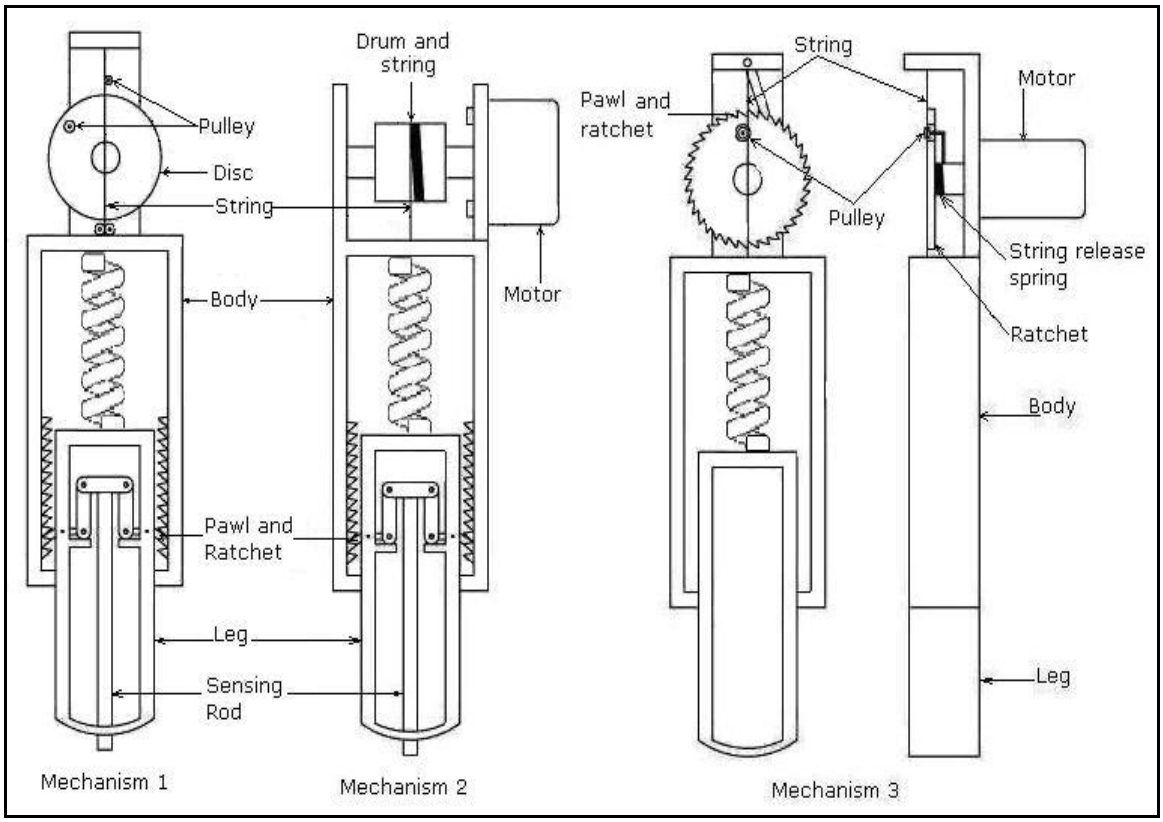

Fig 3.1: Feasible Mechanisms for Energy Pumping

3.2.2 Mechanism 2:

A mechanism 2 uses same kind of latching system, but it differs in method of application of force to pull the string. This method is effective as compared to method used in mechanism 1. The mechanism two consists of drum and string instead of disc and pulley. The drum is directly connected to the actuator shaft. One end of sting is connected to drum and other end is connected to leg through a compression spring (not shown in Fig 3.1). As actuator rotates in flight phase, drum winds the string. The winding of string on the drum results in compression of spring. Spring compression is defined by the actuator rotation. At desired spring compression, motor stops and gets reversed to its original position. Latching and unlatching of pawl and ratchet takes place in same manner as explained in mechanism 1. Again as next flight phase starts, motor rotates and cycle repeats.

3.2.3 Mechanism 3:

A mechanism 3 has same method of effort application as used in mechanism 1. But it has different latching arrangement. This arrangement is results in less energy loss in impact as compared to arrangement in mechanism 1. As mass of leg is reduced due to shifting of pawl and ratchet from leg to body. It consists of a circular ratchet, a pawl, a string, a pulley with crank etc. Ratchet is mounted on the spline shaft to offer horizontal sliding due to string tension against the string release spring as shown in Fig 3.2.

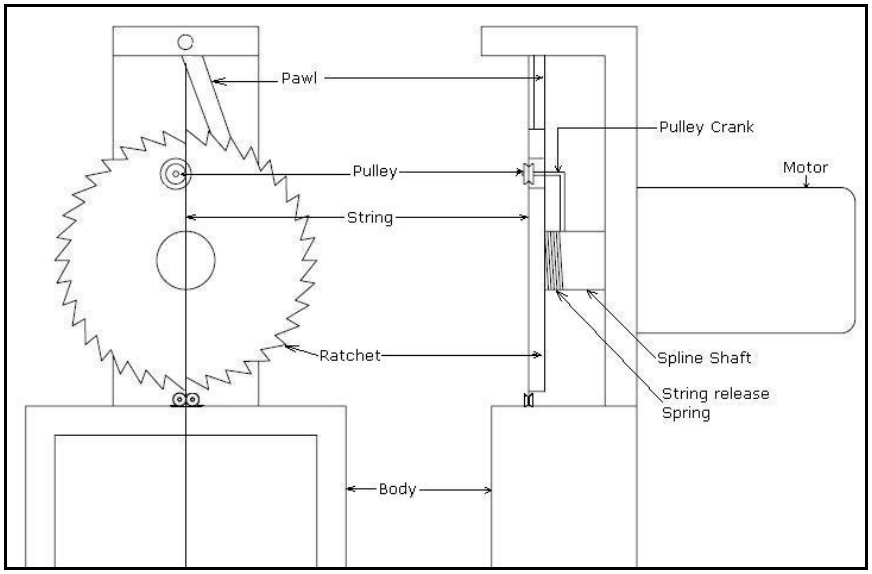

Fig 3.2: Close view of Mechanism 3

Initially string is tight and presses the ratchet against the string release spring. In the flight phase, actuator rotates in clockwise direction results in the compression of spring. The spring is compressed due to engagement of the string in pulley. After the desired compression motor stops and ratchet holds the leg at that position. At touch-down string becomes slack and gets disengaged from the pulley due to string release spring. Now compression spring fully releases its energy to body kinetic energy as it is mechanically disconnected from body. This results in next flight phase. At take-off again tight string forces ratchet disc against string release spring and cycle continues.

3.3 Proposed Mechanism:

Above all mechanism fulfills hopper basic functional requirement. The mechanism 1, 2 and 3 are evaluated against functional requirements and performance parameters. In this evaluation mechanism performance against respective evaluation criteria is graded from number *0* to *5*. Also evaluation criteria carry weights from *0* to *5*. From *0* to *5*, performance of mechanism increases against evaluation criteria and weighting increases importance of criteria as far as hopper performance is concern.

Table 3.1: *Evaluation of Mechanism*

Mechanisms / Criteria	Mechanism 1	Mechanism 2	Mechanism 3
Range of Energy Pumped (*5*)	*2* *(5x2)*	*5* *(5x5)*	*2* *(5x2)*
Efficiency (*4*)	*3* *(4x3)*	*5* *(4x5)*	*3* *(4x3)*
Reduction in energy losses (*3*)	*2* *(3x2)*	*2* *(3x2)*	*4* *(3x4)*
Mechanical Simplicity (*2*)	*2* *(2x2)*	*4* *(2x4)*	*3* *(2x3)*
Total Points	*32/70*	*59/70*	*40/70*

.

From Table 3.1, it is clear that performance of mechanism 2 is better than mechanism 1 and 3. So the mechanism 2 is used for energy pumping of vertical hopper. On experimental set-up motion of hopper is restricted in vertical axis by using guide bars.

Friction loss in guide bars is reduced by designing the hopper symmetrical about vertical axis. So mechanism 2 needs small modifications so that hopper becomes symmetrical about vertical axis.

3.4 Modified Mechanism:

The reason of un-symmetry of vertical hopper with mechanism 2 is actuator mounting. The actuator mounting needs to be change so that hopper becomes vertically symmetric. This can be achieved by mounting the actuator vertically. But same time shaft mounting should remain same. After incorporating bevel gear pair between actuator and shaft, desired effect will be achieved. Fig *3.2* shows the modified energy pumping mechanism for vertical hopper.

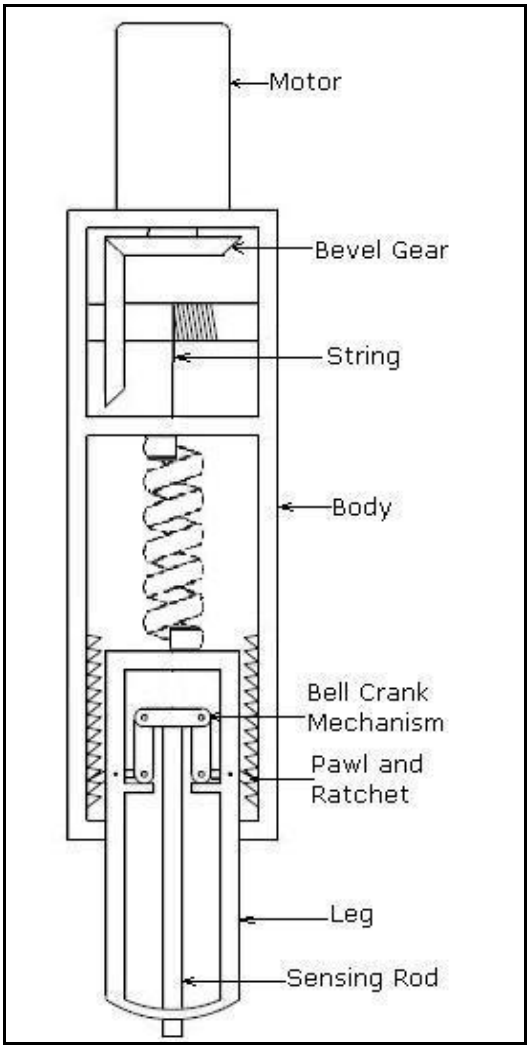

Fig 3.3 Energy Pumping Mechanism for Vertical Hopper

Chapter 4

HOPPER DESIGN

As essential aspect of hopper design is the natural dynamics of the system produces hopping motion. If hopper is dropped, it should bounce several times before falling over. The ideal model of hopper has mechanical stability of body attitude and a mass less leg

4.1 Design Considerations:

The main objective of design is to reduce the overall weight and friction losses. Overall reduction in weight results in reduced energy loss in impact and less energy is required at take-off. The friction losses can be reduced by maintaining proper clearance and reducing normal reaction between mating parts. Lastly hopper can be easily assembled and dissembled.

To achieve these design goals on an experimental set up, hopper leg and body is made from acrylic and set up is symmetrical about vertical axis. Along with this proper clearance is maintained in body and leg. The hopper is vertically guided by *2* LM guides.

4.2 Experimental Set up:

Fig 4.1 shows the experimental set up of vertical hopper. It consists of body, leg, thrust mechanism, vertical guide and base plate. Hopper is guided vertically by using *2* linear motion (LM) guides. A compression spring (not shown in Fig. 4.1) is incorporated between leg and body. To prevent the spring from buckling, an aluminum rod is fixed from leg side. The aluminum rod has length more than the half of the spring length. And from body side, one hollow pipe (not shown in Fig 4.1) of same length as that of rod is fixed. One end of string is connected to aluminum rod and other end is to bevel gear shaft. The thrust mechanism consists of motor mounting module, bell crank mechanism, sensing rod, pawl and ratchet. A mechanical contact switch is provided to sense the touch-down and take-off events. An encoder and reduction gear head is incorporated with actuator. A bevel gear pair is installed between actuator and string winding shaft.

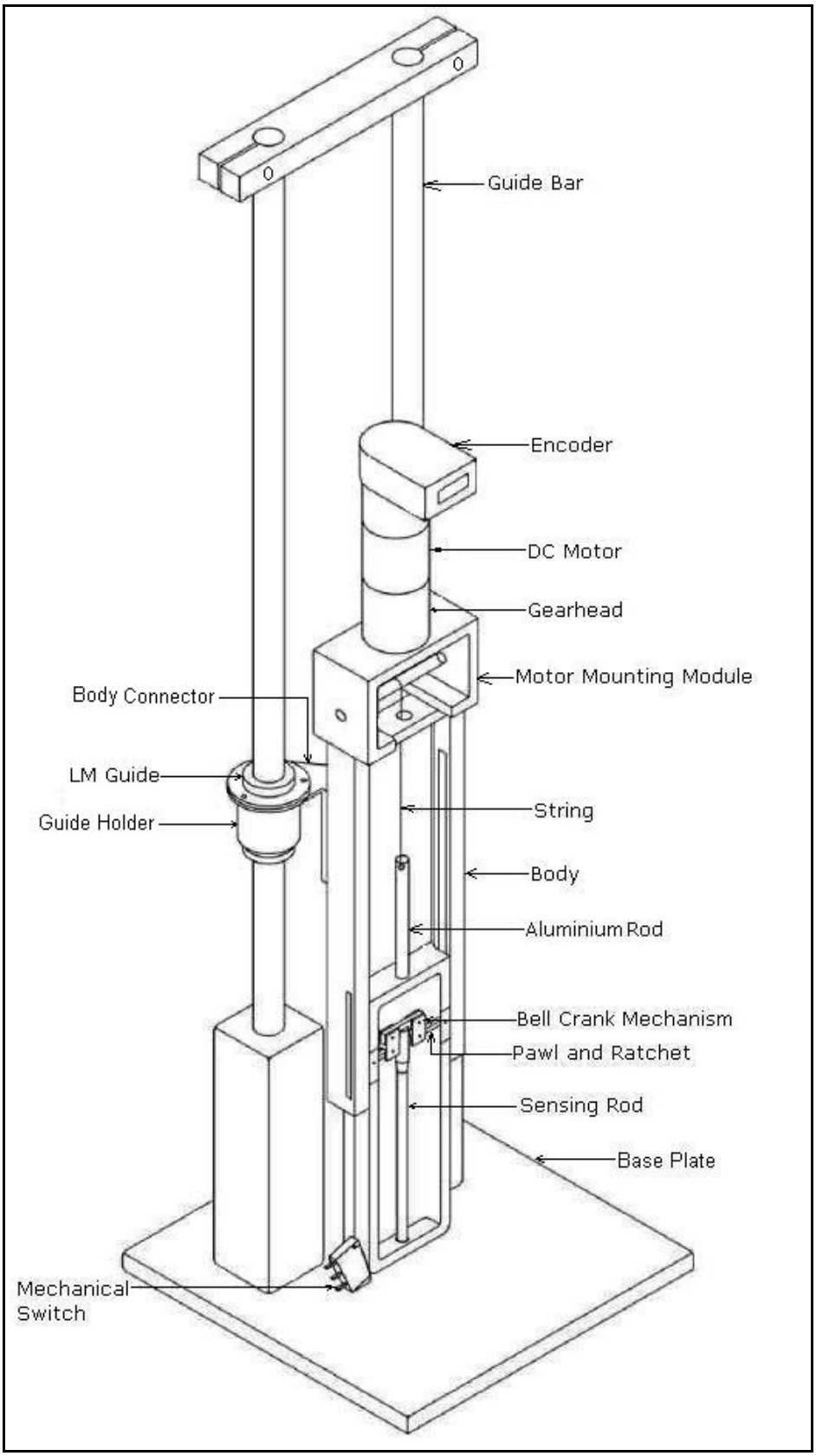

Fig 4.1 Experimental Set-up of Vertical Hopper

4.3 Detailed Design:

It explains part level details of hopper model.

4.3.1 Body:

A hopper body supports the leg, the actuator and LM guides. The leg and body is connected by prismatic pair. At the top edge, body supports the actuator and one lateral side supports the LM guides. Fig 4.2 shows the geometrical parameters of body. It contains slot on inner edges to guide the leg and to provide clearance for pawl. A hole on upper side is to give path to string.

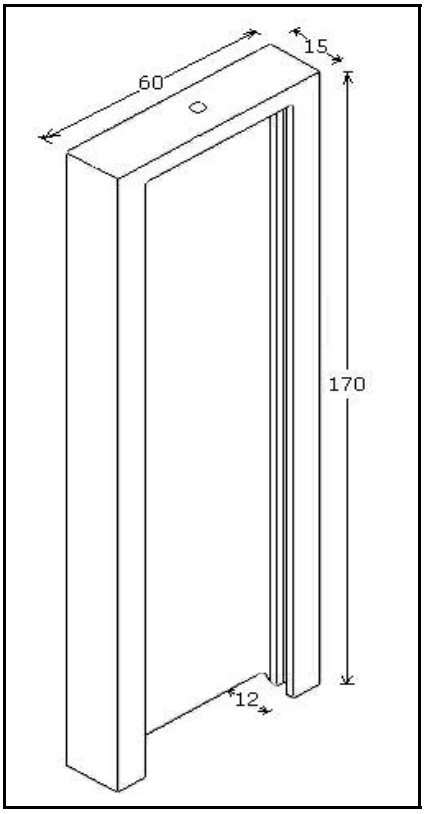

Fig 4.2 Hopper Body

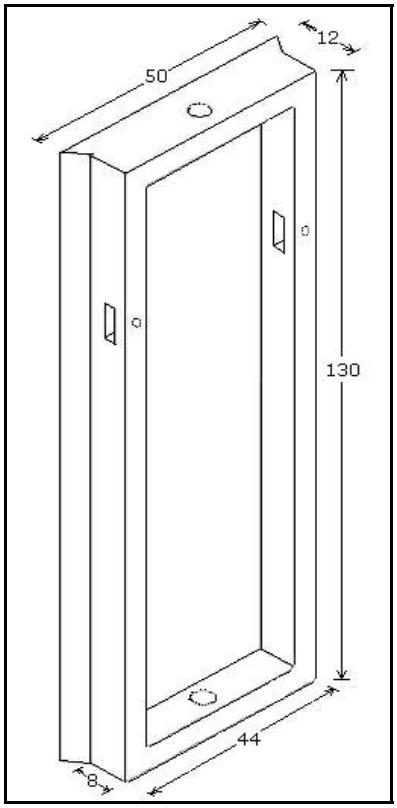

Fig 4.3 Hopper Leg

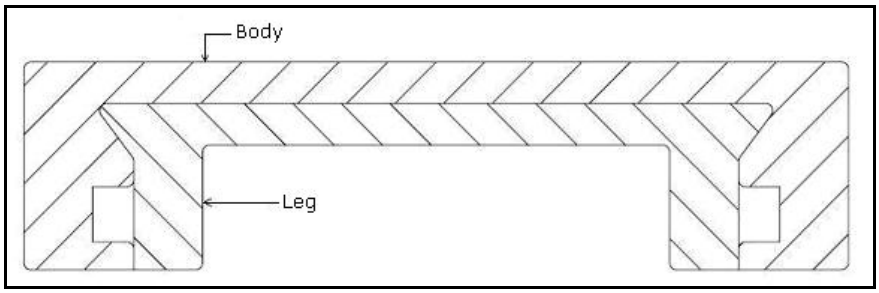

Fig 4.4 Body and Leg cross-section

4.3.2 Leg:

Fig 4.3 shows the geometrical parameters of leg. Outer edges of legs are made such that it maintains enough clearance with body and guide it in vertical direction. Fig 4.4 shows cross section of leg and body (not at pawl and ratchet mounting). In this Fig hollow slot is for pawl and ratchet engagement.

4.3.3 Thrust Mechanism:

Thrust mechanism is used for charging the spring in flight phase and unlatches the pawl and ratchet at touch-down. It consists of the bevel gear pair, string, bell crank mechanism, pawl and ratchet. The bevel gear pair arrangement will discussed in motor mounting module.

4.3.3.1 Pawl and Ratchet:

Pawl and ratchet is latching element of mechanism. The pawl is mounted on the leg and ratchet is fixed on the body. Fig 4.5 shows the pawl dimensions and Fig 4.6 shows line diagram of deflection of pawl so that it get disengaged from the ratchet. Fig 4.7 shows details of ratchet. Ratchet tooth has 2 mm pitch and upper edge makes an angle of 9^{o} with horizontal. This angle reduces the contact force of ratchet at time of touch-down.

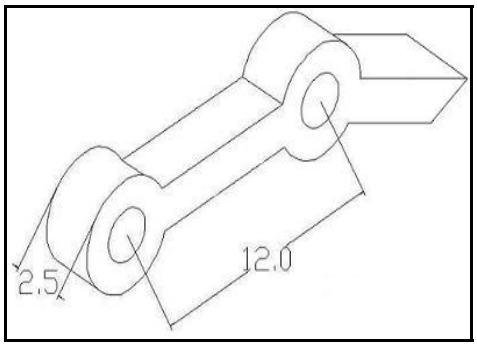

Fig.4.5 Pawl

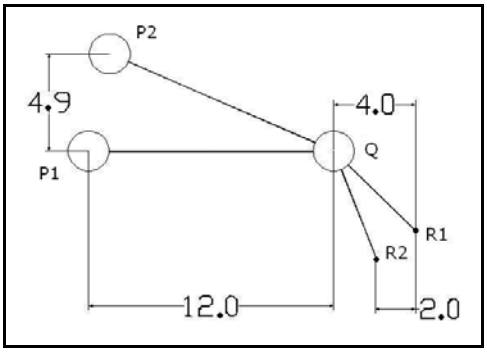

Fig 4.6 Line Diagram of Displacement of Pawl

Pawl Displacement Calculation:

Consider point P, Q and R on the pawl as shown in Fig 4.6. Point Q is pivot point of pawl. Points P_1QR_1 and P_2QR_2 are two positions of pawl. When point R gets horizontal displacement of 2 mm, it disengages the ratchet. Now here assume that 2 mm

displacement of point R moves point P by Δ mm in vertical direction and corresponding angular deflection is ϕ.

Assume that ϕ is small, hence arc length from P1 to P2 is slightly greater that displacement in vertical direction.

$\therefore \Delta = 12\phi$

We know that to unlatch occurs at point, when point R moves by *2* mm horizontally.

$\therefore 2 = QR_1 \cos(45) - QR_2 \cos(\phi + 45)$

$\therefore 2 = 4 - 4\cos(45 + \phi) / \cos(45)$

$\phi = 24.29 \approx 24$

Hence ϕ is 24^o and corresponding vertical deflection of sensing rod is,

$\therefore \ \Delta = 12 \times 24 \times \pi / 180$ *=5 mm*

Therefore to unlatch the pawl, point P should moves by *5 mm* in vertical direction.

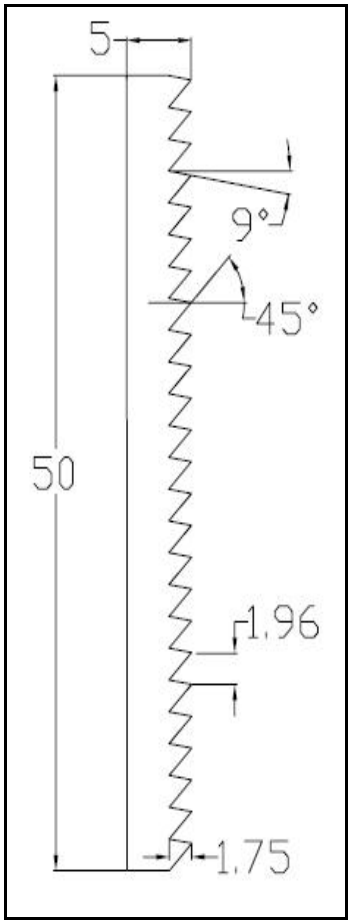

Fig 4.7 Ratchet Details

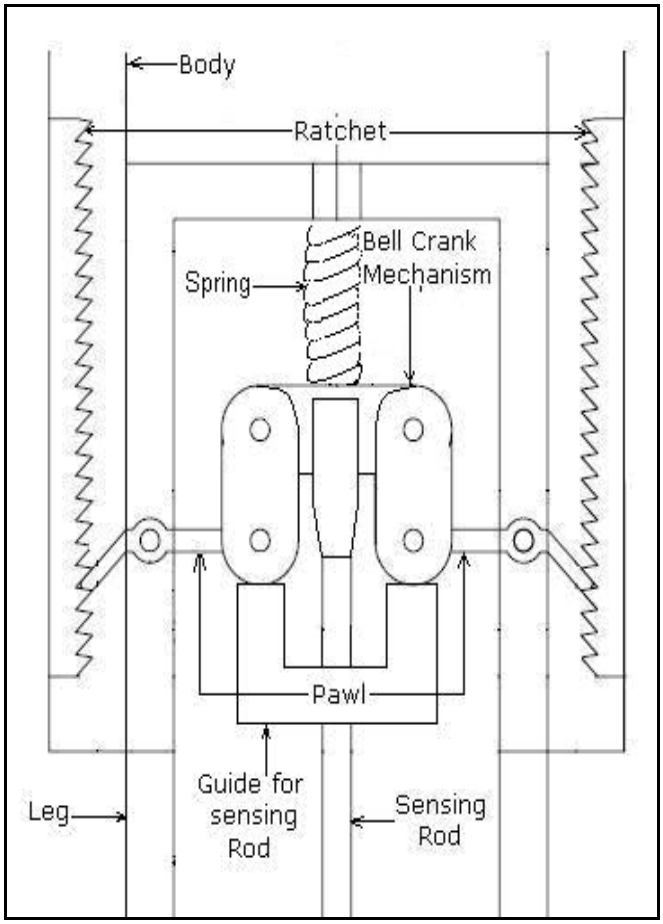

Fig 4.8 Pawl and Ratchet with Bell Crank Mechanism

4.3.3.2 Bell Crank Mechanism:

Fig 4.8 shows the details of bell crank mechanism with pawl and ratchet. It positively connects pawl and sensing rod. Links dimensions of mechanism are as shown in Fig 4.9. Link 2 is connected to sensing rod and link 1 is connected between link 2 and pawl. All links are made from aluminum, so that they have less weight and sufficient strength in tension and bending.

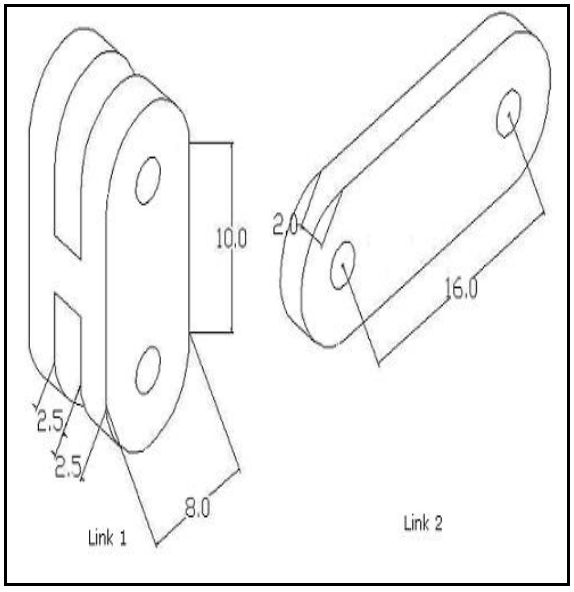

Fig 4.9 Links of Bell Crank Mechanism

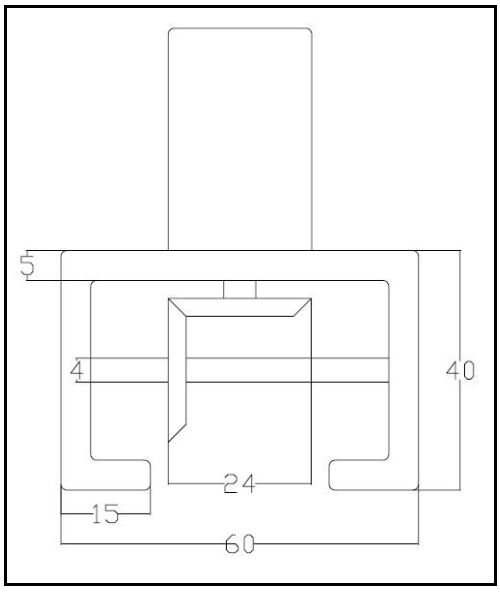

Fig 4.10 Motor Mounting Module

4.3.3.3 Sensing Rod:

Fig 4.8 shows the sensing rod with bell crank mechanism and vertical guide. It is a cylindrical rod, made from aluminum. It drives the bell crank mechanism results in unlatching of pawl. It is vertically guided at two points, one is through the leg and other is small piece of acrylic with the hole. Vertical motion of sensing rod always keep link 2 of bell crank mechanism in horizontal position and results in the equal displacement to both pawls. It extends outside the leg by *5mm* so that pawl is completely unlatched at touch-down. As shown in Fig 4.8, a compression spring is vertically installed between leg and link 2 so that pawl will effectively latch. It has very low stiffness as compared to main spring (k=10-50N/m).

4.3.4 Motor Mounting Module:

It consists of bevel gear pair and actuator assembly. As shown in Fig 4.10, actuator is vertically mounted on upper edge. After fixing the actuator bevel gear is fixed on the actuator shaft. Before mounting the shaft, it is inserted from one side then bevel gear and finally fixed in bearing at other end. Then move the loosely mounted driven gear closer to driver gear and fix it at proper position to ensure proper engagement of teeth. A string with *1* mm diameter is attached to a shaft of bevel gear.

4.3.5 Vertical Guide:

Vertical guide consists of assembly of LM guide, guide holder, body connector and circlips. LM guide consists of a cylindrical tube, containing arrangement of re-circulating balls in longitudinal direction. When a guide bar is inserted in the tube, balls make contact with it. Thus LM guide convert sliding friction into rolling friction. Fig 4.11 shows details of LM guide and holder. The LM guide is made from steel and holder is made of acrylic. The LM guide has two slots on the outer side of tube. These slots are to hold the object with help of internal circlips. In between the circlips, holder is inserted. Before inserting the holder in LM guide, it is assembled with body connector. Body connector is aluminum plate as shown in Fig 4.12, its lateral side connects to the body and top edge is connects to the LM guide. Thus whole assembly guide hopper in vertical direction.

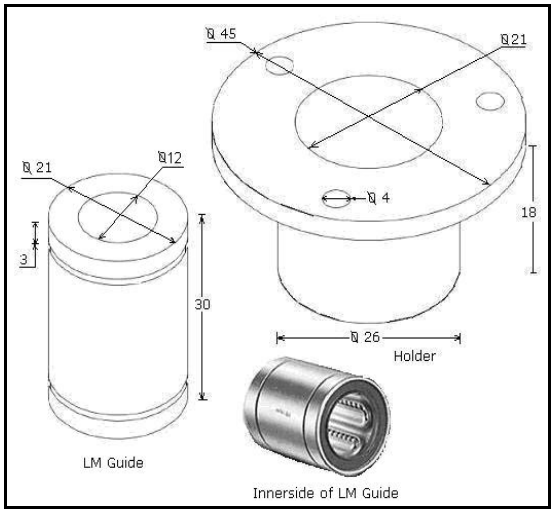

Fig 4.11 LM Guide and Holder

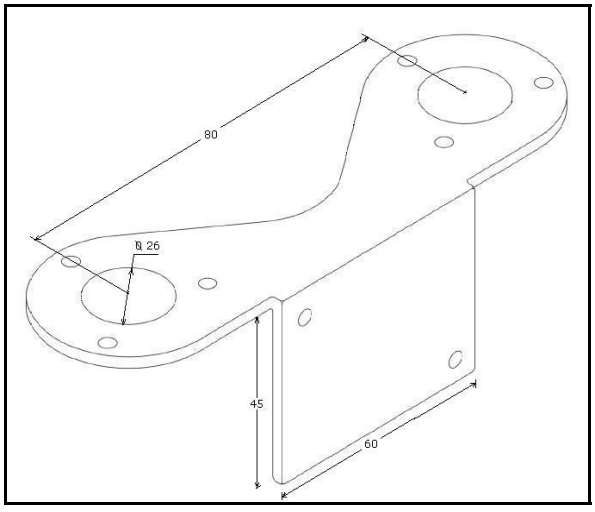

Fig 4.12 Body Connector

4.3.6 Scale and Pointer:

To measure the hopper body position during hopping, a scale is vertically fixed near the guide on the base. A pointer is fixed in the body so that it will slide above the scale and give the body altitude. As it is 1 DOF system, only one reading of system will define the leg position.

4.3.7 Base Plate and Guide Bar:

As shown in Fig 4.1, base plate support the whole set up. Two guide bars are bolted to the base plate so that it will remain vertical to guide the hopper.

4.3.8 Spring:

The standard spring of with our prescribed stiffness and dimension is tough to get. So here we have designed the spring for available material and get manufactured from manufacturer.

Design equations of helical compression spring, under static load of F [11].

$$\tau = K_s \frac{8FD}{\pi d^3} \quad \text{.....4.1}$$

Where, d is the wire diameter, D is mean coil diameter and K_s is a shear stress correction factor given:

$$K_s = \frac{2C+1}{2C} \;;\; C = \frac{D}{d} \quad \text{.....4.2}$$

Now spring rate is given by:

$$k = \frac{Gd^4}{8D^3N} \quad \text{.....4.3}$$

Where N is number of active turns and G is modulus of rigidity of spring material.

For fatigue load with maximum and minimum loading F_{max} and F_{min}, amplitude force and mean force is given by;

$$F_a = \frac{F_{\max} - F_{\min}}{2} \;;\; F_m = \frac{F_{\max} + F_{\min}}{2} \quad \text{.....4.4}$$

The shear stress amplitude and the shear stress mean value is would be;

$$\tau_a = K_B \frac{8F_aD}{\pi d^3} \;;\; \tau_m = K_s \frac{8F_mD}{\pi d^3} \quad \text{.....4.5}$$

Where K_B is Bergstrasser factor which is defined as;

$$K_B = \frac{4C+2}{4C-3} \quad \text{.....4.6}$$

The tensile strength of material is obtained from Ref [12]

$$S_{ut} = \frac{A}{d^p} \quad \text{.....4.7}$$

Where *A* and *p* are material parameters and is given in following table.

Table 4.1 Spring Material Tensile Strength

Material	*p*	*A (kpsi)*
Music wire	*0.163*	*186*
Oil tempered wire	*0.193*	*146*
Hard drawn wire	*0.201*	*137*
Chrome vanadium	*0.155*	*173*
Chrome silicon	*0.091*	*218*

The maximum allowable torsional stress is about half of the tensile strength [12].

Some other parameters of square and ground compression spring is obtained by,

End coils: $N_e = 2$

Total coils: $N_t = N+2$

Free Length: $L_0 = pN+2d$

Solid Length: $Ls = dN_t$

Pitch: $p = (L_0-2d)/N$

Now design requirement for hopper model are;

Spring constant: $k = 1000N/m, 2000N/m$

Max Outer Diameter: $D_0 = 12mm$

Free Length: $L_0 = 120mm$

Among the available materials, Oil tempered wire is selected for our design.

Design of one spring is explained in detail and final design of other spring will be given in Table *4.2*.

For $k = 2000\ N/m$ with coil diameter $d=1.5mm = 0.059inch.$

Other parameters, $D_0 = 12mm;\ D = D_0 - d = 10.5mm$

$$N = 22.24 \Rightarrow N = 23 \qquad N_t = 25; \qquad p = 5.5mm \text{ and } \quad L_s = 37.5mm$$

Above all parameters are related to dimensional analysis of spring. Now stress analysis of spring is given by,

$$S_{ut} = 252.057\ x10^3\ psi = 1737.877MPa$$

$$\tau_{all} = 868.938MPa$$

$$K_s = 1.07;\ K_B = 1.2;\ C = 7$$

Allowable Static Load = *110.7463N.....from Eq4.1*

Allowable Fatigue Load = *98.758N.....from Eq4.5*

This designed spring is tested for stiffness under tensile loading and unloading. Fig 4.13 shows the displacement variation of spring for every change in load of *100*grams. The designed spring gives the experimental spring rate of *2450N/m*. But after increasing the number of turns up to *28* it gives spring rate of *2000N/m.* This may happen because some difference in material properties, manufacturing errors or something goes wrong in hardening process.

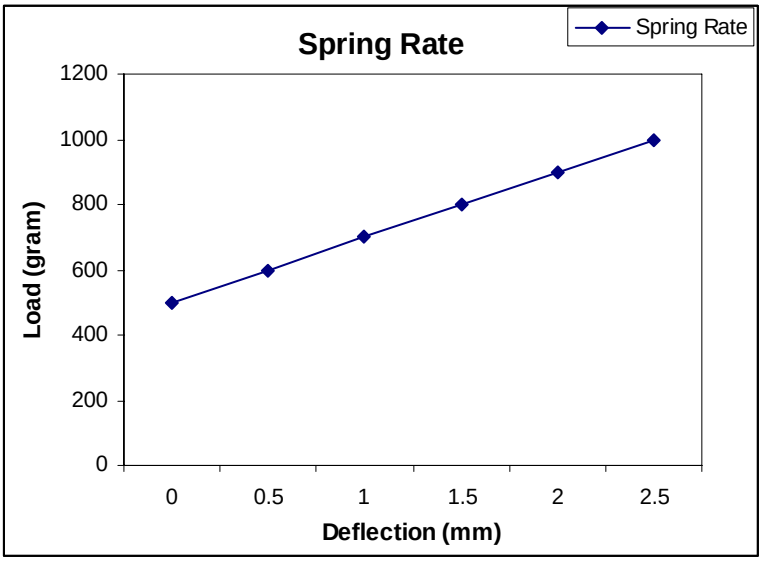

Fig 4.13: Spring Test under Tensile Loading and Unloading

Table 4.2 shows the detailed spring specifications.

Table 4.2: Spring Specifications

Spring Rate (*N/m*)	*1000*	*2000*
Wire Diameter (*d*) *mm*	*1*	*1.5*
Coil Diameter (*D*) *mm*	*7*	*10.5*
Total Number of turns (N_t)	*32*	*25*
Free Length (L_0) *mm*	*120*	*120*
Pitch (*p*) *mm*	*4*	*5.5*

4.4 Energy Analysis:

In hopper, energy sources are mass of different parts and spring stiffness. For that we need mass of body parts and leg parts as the spring rate is known to us. These masses are measured on electronic weighing machine.

Mass of hopper body includes mass of body, ratchet, motor mounting module, LM guide, guide holder and body connector. That of un-sprung mass (mass of leg parts) includes mass of leg, pawl, sensing rod, sensing rod guide, bell cranks mechanism and rod used for guiding the spring.

Mass of body parts (*M*) = *510 grams*

Un-sprung mass (*m*) = *63 grams*

In order to select the actuator on the basis of energy losses, energy analysis is done for steady state hopping with spring of *2000 N/m.*

Hopper motion is divided into four phases as shown in Fig. 4.14;

I. From apex point to touch-down.
II. From touch-down to mid-stance.
III. From mid-stance to take-off.
IV. From take-off to apex point.

Parameter related to energy analysis of hopper:

Δh = Change in body position in Y direction from apex point to touch-down.

V_1 = Velocity of body and leg at touch down.

E_{f1} = Energy loss in guide friction from apex point to touch-down

E_1 = Energy loss in impact between leg and ground at touch-down.

E_{f2} = Energy loss in guide friction from touch-down to mid-stance.

δ = Spring compression needs for steady state hopping.

x = Spring compression due to change in body energy from touch-down to mid-stance

E_{f3} = Energy loss in guide friction from mid-stance to take-off.

V_2 = Velocity of body just before take-off.

V_3 = Velocity of body and leg just after take-off.

E_2 = Energy loss in impact between leg and body at take-off.

E_{f4} = Energy loss in guide friction from take-off to apex point.

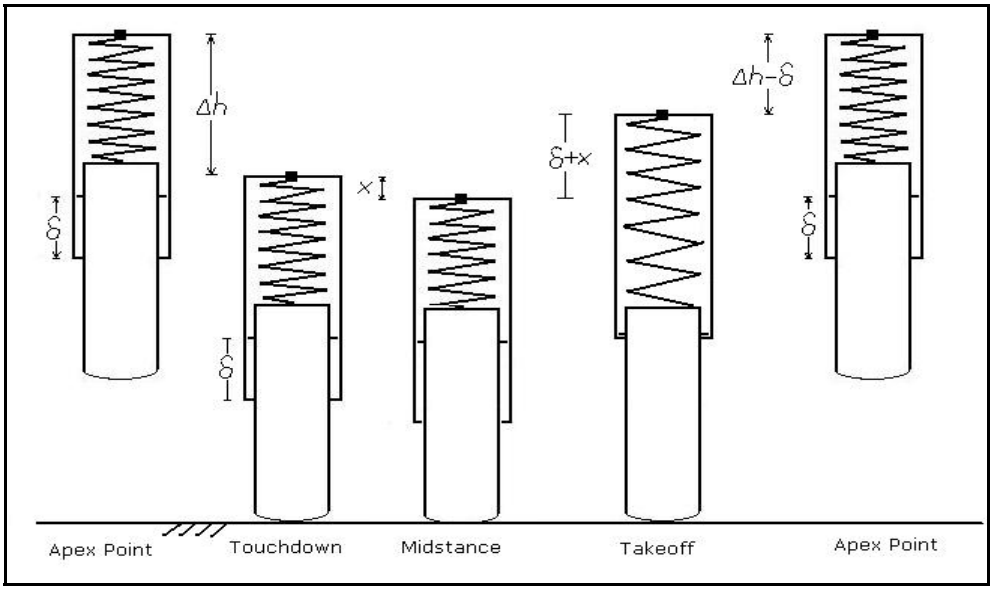

Fig 4.14: Hopper Body Position in Stance and Fight Phase

I. From apex point to just before the touch down:

At apex point hopper content maximum PE. It comprises body and leg PE. This PE gets converted in KE of body and leg at touch down. So energy equation from apex point to just before touch-down is;

$$(M+m)g(\Delta h) = 0.5(M+m)V_1^2 + E_{f1} \quad \text{.....4.8}$$

Now energy change from just before and after touchdown is;

$$0.5(M+m)V_1^2 = 0.5MV_1^2 + E_1 \text{ ……..……} 4.9$$

$$\therefore E_1 = 0.5mV_1^2 \text{ ……..……...} 4.10$$

II. From touch-down to mid-stance:

$$0.5MV_1^2 + Mgx + 0.5k\delta^2 = 0.5k(\delta + x)^2 + E_{f2} \text{ ……..……} 4.11$$

III. From mid-stance to just before take-off:

$$0.5k(\delta + x)^2 = 0.5MV_2^2 + Mg(\delta + x) + E_{f3} \text{ ……..……} 4.12$$

At take-off point, velocity change due to momentum conservation.

$$(M+m)V_3 = MV_2 \text{ ……..} 4.13$$

Energy change just before and after take-off:

$$0.5MV_2^2 = 0.5(M+m)V_3^2 + E_2 \text{ ……..……..…} 4.14$$

$$\therefore E_2 = 0.5\{MV_2^2 - (M+m)V_3^2\} \text{ ……..……..……..} 4.15$$

IV. From take-off to apex point:

$$0.5(M+m)V_3^2 = (M+m)g(\Delta h - \delta) + E_{f4} \text{ ……..…..} 4.16$$

And finally energy balance equation is;

$$E_1 + E_2 + E_{f1} + E_{f2} + E_{f3} + E_{f4} = 0.5k\delta^2 \text{ ……..……} 4.17$$

For energy calculations from experimental readings, initially neglect E_{f2} and E_{f3} to estimate energy loss in hopping cycle for particular spring pre-compression. This analysis also predicts velocity at touch-down and take-off, hopper apex and mid-stance point.

For this hopper, maximum pre-compression is assumed to be *30mm*. From ADAMS simulation for *10mm* pre-compression gives flight time of *0.2sec*. This simulation is on the basis of minimum pre-compression that drives the hopper to steady state hopping height of *35mm*. It also takes care of both; guide and hopper friction losses with static friction coefficient *0.4* and dynamic friction coefficient is *0.3* with preload of *3.5N*. Now considering actual time for spring compression is *0.1sec*. Therefore hopper needs actuator which compress the spring with by *30mm* in *0.1sec*.

4.5 Actuator and Gear head Selection:

A load on actuator is winding a string which is subjected to a continuously increasing force. Total deflection of string is *30mm* in *0.1sec* and motor should get reversed same displacement in *0.08sec* with no load condition. As total flight time is maximum *0.2sec*. For this application DC motor will work with fairly.

Power required for this application is;

Spring PE $= 0.5k\delta^2 = 0.9J$.

This energy is pumped in *0.1sec*, therefore power at load end = *9watts.*

To calculate the power required at motor end, consider motor efficiency, gear-head efficiency and mechanical efficiency of mechanism as *80%,* 85% and *75%* respectively.

Therefore desired actuator power is

$$Power = \frac{9}{0.8 \times 0.85 \times 75} = 17.64W \approx 18W \quad \text{.....4.18}$$

Maximum motor torque:

Torque at gear shaft end is $T_l = F \times r = 60 \times 2.5 = 0.15Nm$

Torque at motor shaft is $T_m = 0.15 / G$ *4.19*

Where *G* is gear reduction ratio.

Maximum Motor speed:

Linear displacement = *30mm*, and time is *t = 0.08sec*

Number of revolution of gear shaft is; $n = \frac{30}{2\pi \times 2.5} = 1.91 \approx 2$ revolutions.

Angular speed at gear shaft end, $N_l = 2 / 0.08 = 25rps = 1500rpm$

Angular speed at motor shaft end,

$$\therefore N_m = (1500 \times G)rpm \quad \text{.....4.20}$$

For selecting the DC motor and gear-head for the given application [14], motor should satisfy following criteria;

1. The root-mean square value of the required motor torque has to be lower than the motor's continuous torque rating (T_c),
2. The required peak motor torque has to be lower than the motor's peak torque rating (T_p)

3. The required peak motor speed has to be lower than the maximum allowed speed of the motor ($N_{m,\,max}$).

In gear-head selection important parameters are input speed, efficiency, torque rating, gear ratio and inertia reflected on motor shaft. The performance of planetary gear is good over conventional gear with spur or helical. As the mass and inertia for three wheel planetary gears is lower than equivalent pinion gear wheel configuration.

Now first selecting gear-head, we can calculate the motor output parameters. If we iterate the gear-head selection, a gear ratio from *3* to *4* offers a feasible values of motor output parameters.

For gear ratio $G = 3$;

$N_m = 4500rpm,\ T_m = 0.05Nm$……...…...From equation *4.19* and *4.20*

For gear ratio $G = 4$;

$N_m = 6000rpm,\ T_m = 0.0375Nm$……...From equation *4.19* and *4.20*

Motor is selected for output torque based on $G = 3$ and output speed based on $G = 4$. Therefore motor output requirements are $N_m = 6000rpm,\ T_m = 0.05Nm$.

Final motor is selected among available motors. To satisfy above requirements, motor selected is *24V* DC micro-motor with planetary gear-head attached to it having a gear ratio 3.71. For the detail specifications of motor and gear-head see the Appendix B.

Apart from this, if we checked for above mentioned criteria [14];

For $G = 3.71$; $T_{RMS} = 0.02475Nm$ (see Appendix B) but continuous motor torque $T_c = 0.0339Nm$. Motor peak torque is *0.139Nm* and required torque is; $T_m = 0.04043Nm$. Lastly, motor continuous speed is *5565 rpm* and maximum allowable speed is *6000rpm*.

Chapter 5

CONTROLLER DESIGN

5.1 System Modeling:

Vertical hopper is the dynamical system and changes its characteristics in stance and flight phase. This change is translated one phase to other phase by touch-down and take-off events. As explained in the hopper design, the DC motor is used to compensate the energy losses in hopping cycle. The DC motor winds the string. This results in spring compression and before mid-stance motor should come to its original position. Minimum time available to achieve this task is *0.1sec* and *0.08sec* respectively.

5.2 Control System Components:

The components of hopper control system include DC motor, Sensors (Encoder and Proximity Sensor), Computer, dSPACE controller board and Pulse Width Modulation (PWM) amplifier. Following text discusses in detail of major components.

5.2.1 DC Motor:

The DC motor details are discussed in section 4.5 and specifications are given in Appendix B.

5.2.2 Sensors:

To sense the motor current position and to detect the take-off/touch-down events, hopper incorporates 2 sensors.

5.2.2.1 Angular Encoder:

The incremental shaft encoder in combination with the DC motor is designed for indication and control of both, shaft velocity and direction of rotation as well as for positioning. A LED source and lens system transmits collimated light through a low inertia metal disc to give two channels with 90° phase shift. The single 5 volt supply and

the two or three channel digital output signals are interfaced with a 5-pin connector (see Appendix B). This encoder is directly connected to motor shaft before gear-head.

5.2.2.2 Proximity Sensor:

To detect the hopper events, contact type proximity sensor is used. Basically it is lever operated mechanical switch as shown in Fig *5.1*. It has 3 terminals, one is used for +5V supply and other is taking output as per application requirement. These two terminals are normally closed (NC) and normally open (NO). When lever is pressed by hopper leg, output of normally open changes from 0V to +5V and normally closed changes from +5V to 0V.

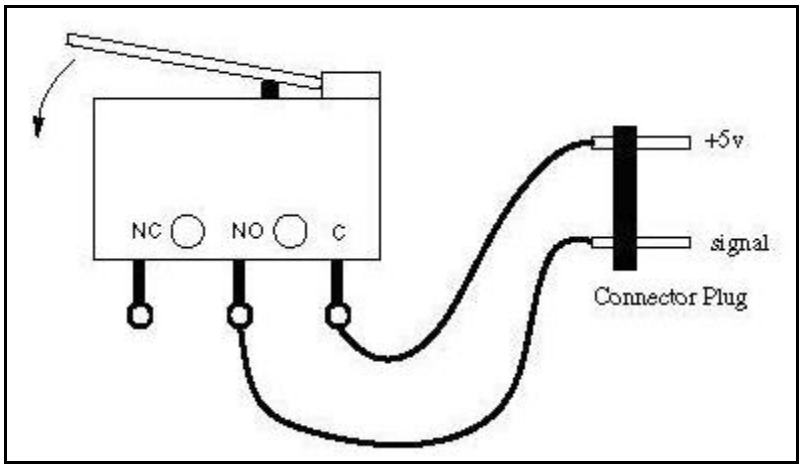

Fig 5.1: Mechanical Switch with Connection

5.2.3 dSPACE Controller Board (dSPACE1104):

The control algorithm is executed on the dSPACE DS1104 R&D controller board. The system includes high speed A/D and D/A boards, a 603 PowerPC floating-point processor running at 250MHz, and a TMS320F240 DSP micro controller. The control algorithms are developed in MATLAB Simulink, converted to C code with the Real Time Workshop, and downloaded to the DSP. In addition to real-time execution of control algorithms, dSPACE allows for real-time parameter updates and monitoring of system signals. This flexibility offers to change the pre-compression during the hopping.

5.2.4 PWM Amplifier:

The amplifier used for motor control is voltage control amplifier. Basically it has control PWM duty hence motor voltage. It has 2 bits, called as IN A and IN B which decided the direction of rotation of amplifier.

5.3 Controller Design:

The Functional requirements of controller are-

1. Continuously sense the motor position control and works out the difference between the actual measured position and the required position.
2. Some way of converting the position error into a variable duty-ratio pulse width modulation (PWM) to give a controllable average voltage at the motor

To achieve the above functional requirement of motor position control algorithms is developed in MATLAB Simulink. After building the program, all necessary programs for motor control and real time interface are generated on dSPACE controller board. Fig 5.2 shows the control system outline for hopper model.

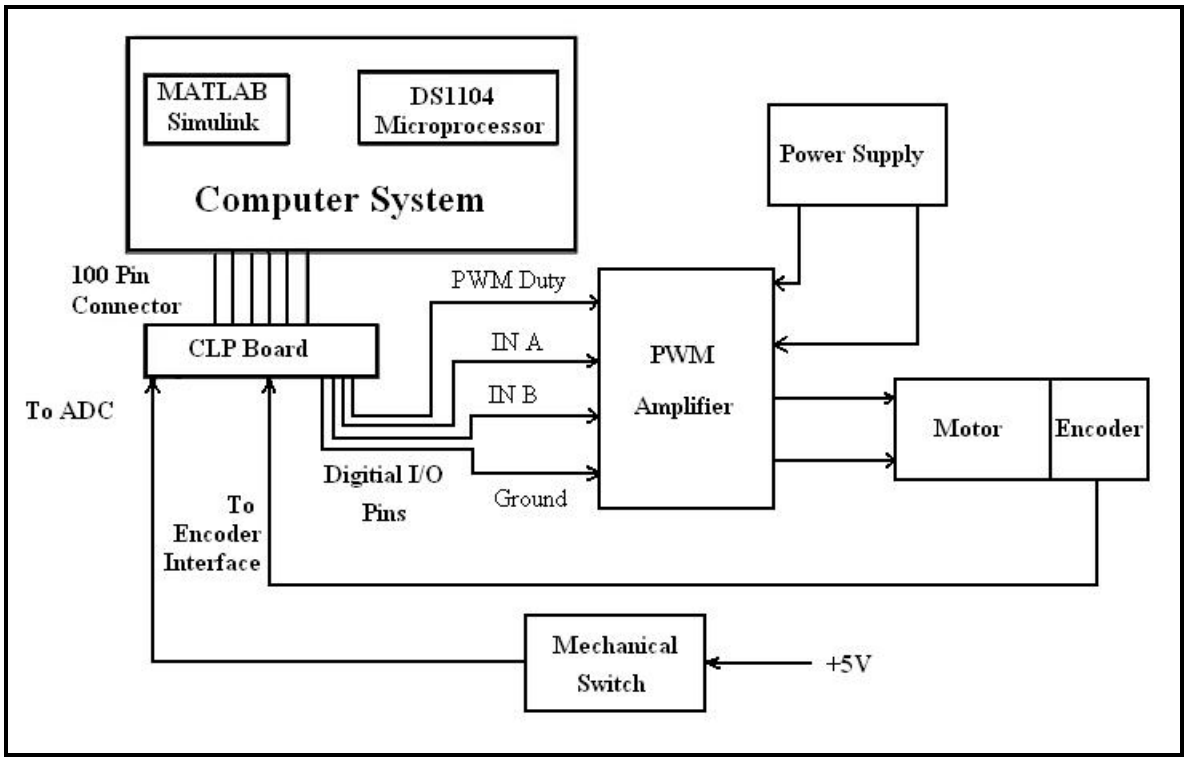

Fig 5.2: Hopper Control System

5.3.1 Control Algorithm:

1. Start the artificial clock as soon as output of mechanical switch goes low.
2. Define motor desired position by mathematical function on the basis of this time. While defining function, take care of time (T) so that motor should return to its original position before mid-stance. Here motor forward and reverse position is defined by function; $0.5A\{1-\cos(\frac{\pi}{T_f}t)\}$ in [*0, T_f*] and $0.5A\{1+\cos\{\frac{\pi}{(T-T_f)}(t-T_f)\}\}$ in [T_f, T], where A is amplitude of oscillation, T_f, and T are forward and cycle time.
3. Compare the desired and actual motor position values. On the basis of error between this values PID controller will generates output. The modulus of the controller output decides the PWM duty and sign will decide the bit values of IN A and IN B bit, hence direction of rotation of motor.

Once above three steps are executed motor comes to its original position. Again next take off resets the artificial timer, motor gives one oscillation in the specified time and cycle continues.

Chapter 6

EXPERIMENTAL RESULTS AND DISCUSSION

For the designed set up, experiments are conducted to study steady state hopping for different spring pre-compression. For each spring pre-compression, corresponding maximum height and minimum height is measured with the help of scale and pointer.

6.1 Experimental Results:

As hopper stops within *7-8* hops for pre-compression below *16mm*, experiments are conducted for *5* readings starting from *16mm* to *24mm.* Following table shows detailed analysis for steady state hopping. Before starting the experiment, the equilibrium position of hopper is noted with the help of a pointer. The other hopping parameters are found using the method described in section *4.4*. To simplify the analysis, initially neglect E_{f2} and E_{f3} to find V_1, V_2, E_1, E_2, E_{f1} and E_{f4}. Then check the feasible values of the energies by finding neglected losses as a positive number. That is, subtract all the energy losses from energy added. If it doesn't give a positive number, then divide the reminder of subtraction in to two parts such that larger part will be subtracted from E_2 and smaller part will be added in E_1. As energy losses from mid-stance to take-off will be greater than from touch-down to mid-stance. Based on the new values of E_1 and E_2 find V_1 and V_2 again continue till for all reading, subtraction becomes positive number.

6.1.1 Observations:

Table 6.1 Experimental Readings and Velocity Analysis

δ (mm)	h_{max}	h_{min}	h_{eq}	ΔH (mm)	x(mm)	V_1 (m/s)	V_2(m/s)
16	208	173	190	35	1	0.4686	0.7559
18	210	172	190	38	1.5	0.56077	0.922
20	214	170	190	44	2	0.6537	1.0857
22	220	166	190	54	2.5	0.7473	1.2473
24	231	165	190	66	3	0.8401	1.4087

Table 6.2 Hopper Energy Analysis from Experiment

δ (mm)	E_1 (J)	E_2 (J)	E_{f1} (J)	$E_{f2}+E_{f3}$ (J)	E_{f4} (J)	E_f (J)
16	0.007137	0.01647	0.1286	0.07608	0.02771	0.23239
18	0.01022	0.02450	0.1239	0.08593	0.07945	0.28928
20	0.01389	0.033976	0.12532	0.09557	0.13124	0.35213
22	0.01815	0.04484	0.1328	0.10554	0.18267	0.42101
24	0.02294	0.057195	0.1637	0.11636	0.21758	0.49764

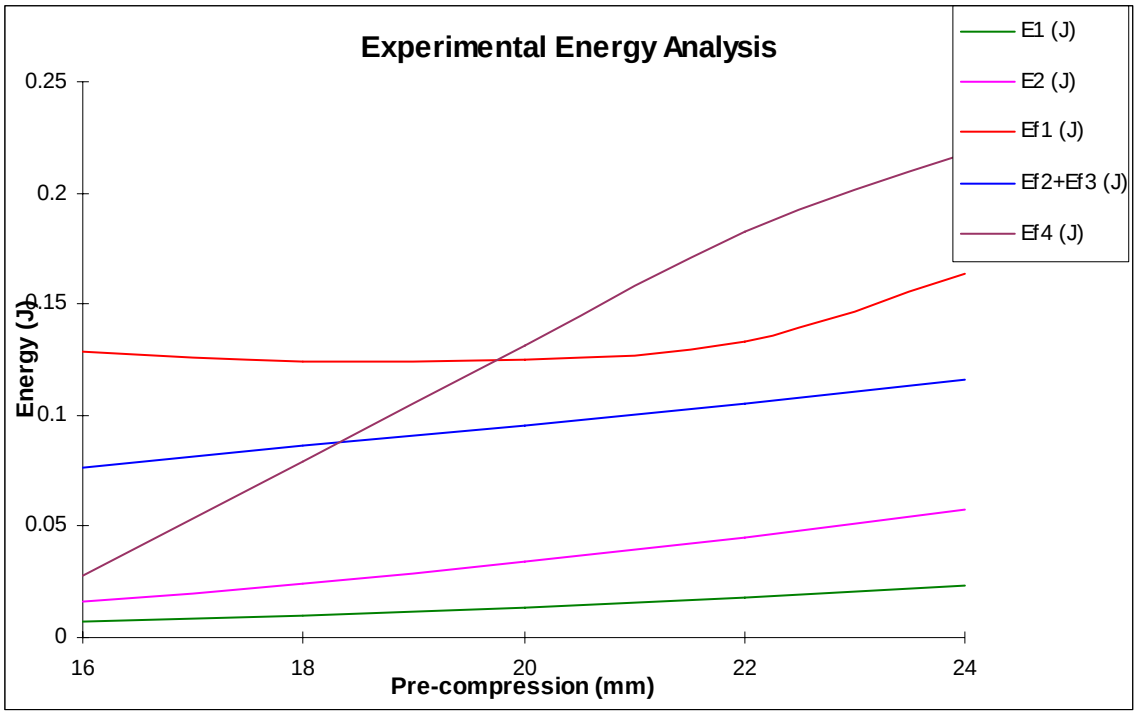

Fig 6.1 Experimental Energy Analysis

Table 6.3: Observation from Experimental Calculations

δ (mm)	$\Delta h = (h_{max} - h_{eq} + \delta)$ mm	Time to reach ground T_1 sec	(E_{f1}/T_1)
16	34	0.0832	1.54567
18	38	0.08801	1.40779
20	44	0.09471	1.3232
22	52	0.102963	1.2897
24	65	0.1151	1.422

Figure 6.3 shows the experimental set up used for study of steady state hopping robot. Table 6.2 shows the different energy losses per hop on the experimental model. The plot in Fig 6.1 shows the variation of energy loss with pre-compression, here all energy losses increases with the pre-compression in different proportion. It is clear from the Table 6.3, energy loss (E_{f1}) per unit time required from apex point to touchdown is remains constant. As compared to other energy loss, rate of increase of E_{f4} is quite higher. This is because for a less spring compression, less spring force exerts on the body at the time of take-off. Moments due to this spring force may be balanced by moments due to weight. As spring pre-compression increases, it increases spring force and moments due to this force dominates over the moments due to weight. So there is drastic energy loss occurs in small time interval.

6.2 ADAMS Simulation Results:

The hopper model is simulated in ADAMS to give the same hopping height for the specified pre-compression. Fig 6.2 shows hopper model in ADAMS simulation package. It has same masses and spring stiffness as that of experimental model. Here actuator is replaced by a force function which triggers when body crosses a specified distance from ground. Hopper is guided in vertical direction by defining a prismatic pair between guide bar (attached to ground) and hopper body. A Mechanism spring is defined between the bell crank mechanism and leg, so that it will positively latch the pawl. It has very low stiffness ($k= 10N/m$)

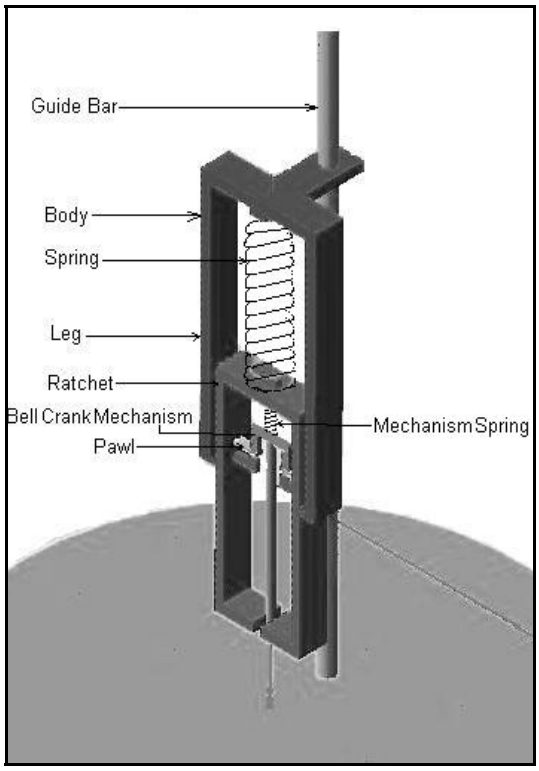

Fig 6.2: Hopper Model in ADAMS

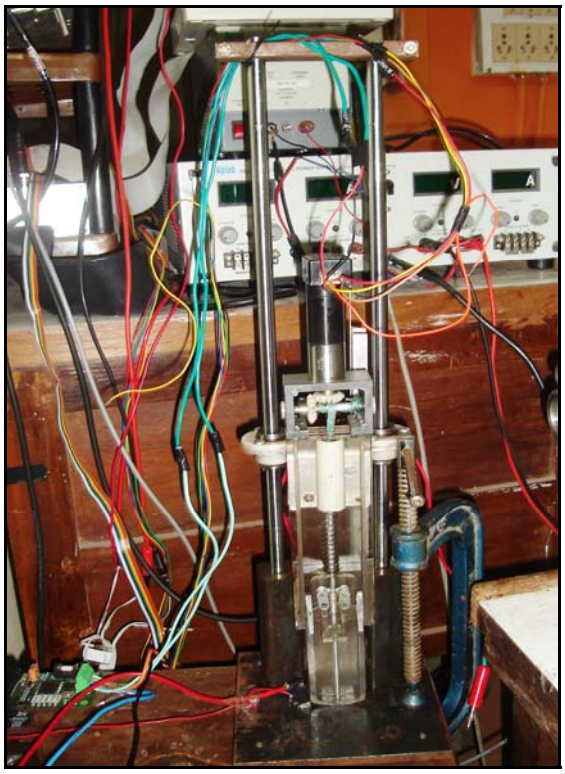

Fig 6.3: Experimental Model of Hopper

6.2.1 ADAMS Simulation Plots:

Fig 6.4 shows the variation of body and leg position with respect to time in steady state hopping and Fig. 6.5 shows body and leg velocity is plotted on the leg position plot separately so that we can read body and leg velocity at two events. In Fig 6.5 points *A* indicates the maximum negative velocity attained body and leg in flight phase. Velocity variation from point A to B is due to sensing rod. Stance phase starts fro point B to C as leg velocity is zero for this time interval. In this interval it is clear that after the leg body reaches zero velocity. Point D and C is take-off point At this point velocity of body is suddenly reduced from maximum value. A sharp increase in curve DFG is due to pulling of leg in flight phase. From G to A, leg and body moves with same velocity. At take-off leg velocity shows sharp rise and fall, this is because impact occurs between leg and body and it takes small time to settle-down.

This plots is for $\delta = 16mm$ and $\Delta h = 35mm$. In the same way plots are taken for each reading to get the velocity at touch-down and take-off point. To model the friction on actual setup, choose the friction coefficient and preload so that for the same pre-

compression it gives approximates hopping height. Table 6.4 and 6.5 shows reading of important parameters and hopper energy analysis from ADAMS simulation.

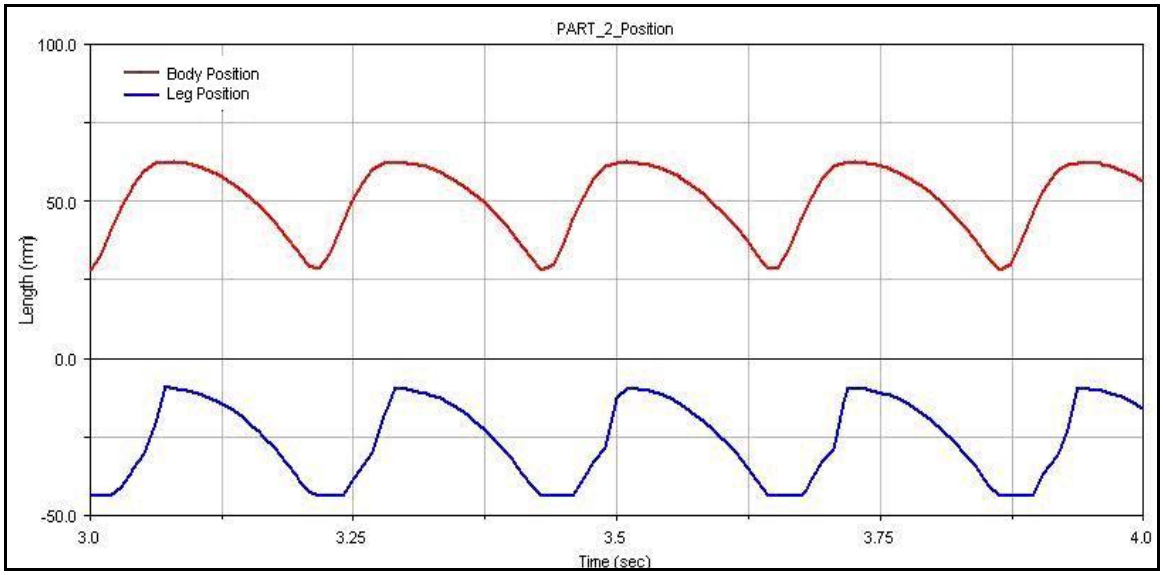

Fig 6.4: Body and Leg Position Vs time

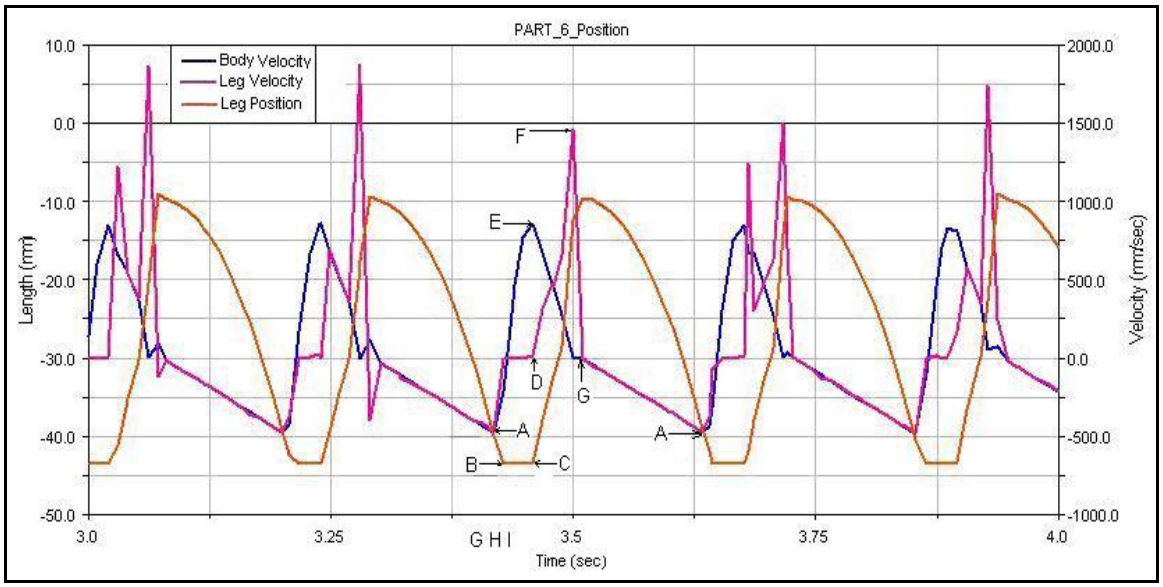

Fig 6.5: Body and Leg Velocity Vs time

Table 6.4: Reading from ADAMS Simulation

δ (mm)	ΔH mm	μ_s	μ_d	Friction Force Preload (N)	V_1 m/s	V_2 m/s	T_s sec	T_f sec
16	35	0.4	0.3	3.0	0.510	0.850	0.0314	0.185
18	40	0.4	0.3	3.0	0.620	0.960	0.0314	0.19
20	46	0.4	0.3	3.0	0.650	0.985	0.0351	0.191
22	55	0.4	0.3	3.0	0.710	1.115	0.0351	0.2120
24	68	0.4	0.3	3.0	0.784	1.262	0.0350	0.2348

Table 6.5: Hopper Energy Analysis from ADAMS Simulation

δ (mm)	E_1 (J)	E_2 (J)	E_f (J)
16	0.008453	0.02083	0.2267
18	0.01249	0.02657	0.28494
20	0.01373	0.02796	0.35831
22	0.01638	0.03584	0.43178
24	0.01997	0.04591	0.51012

6.3 Comparison of Experimental Results with ADAMS Simulation Results:

As we have modeled the hopper in ADAMS for same parameters. Here experimental height for respective pre-compression is achieved by modeling the guide friction in ADAMS. This simulation results are compared with experiment model. Following graph shows the variation of energy losses from ADAMS simulation and experimental calculations. Subscript ‘A’ and ‘E’ indicates that ADAMS and experimental results respectively.

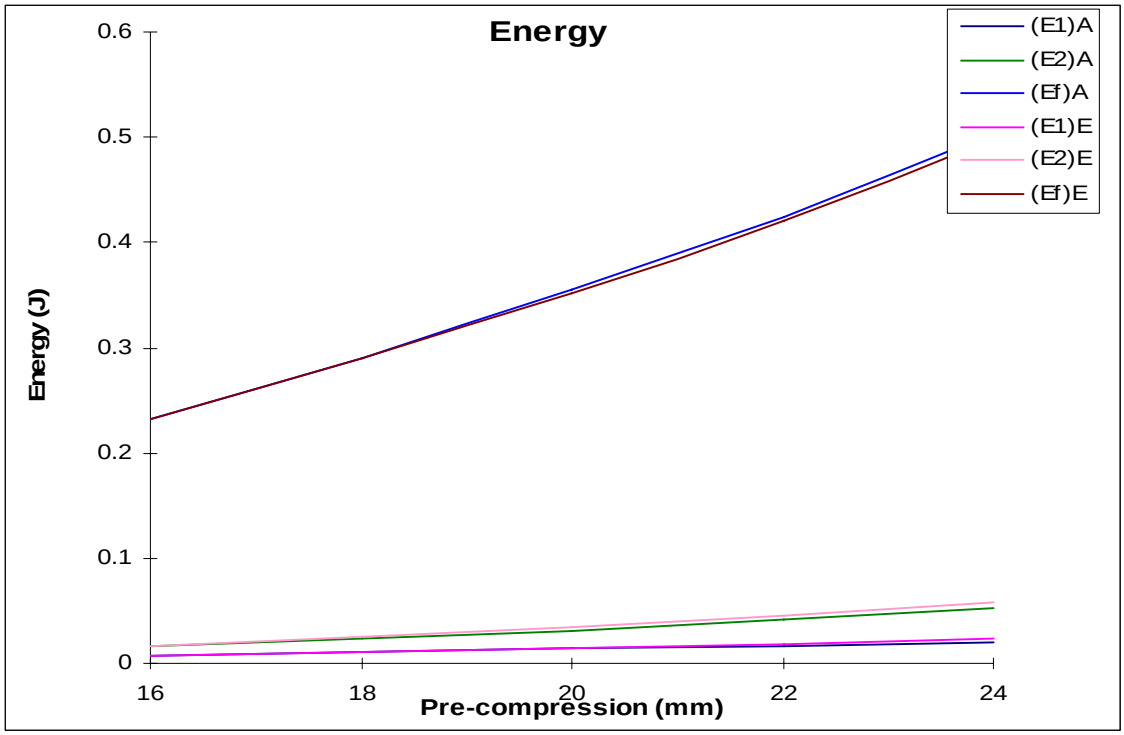

Fig 6.6: Comparison of Hopper Energy Losses from ADAMS and Experiment

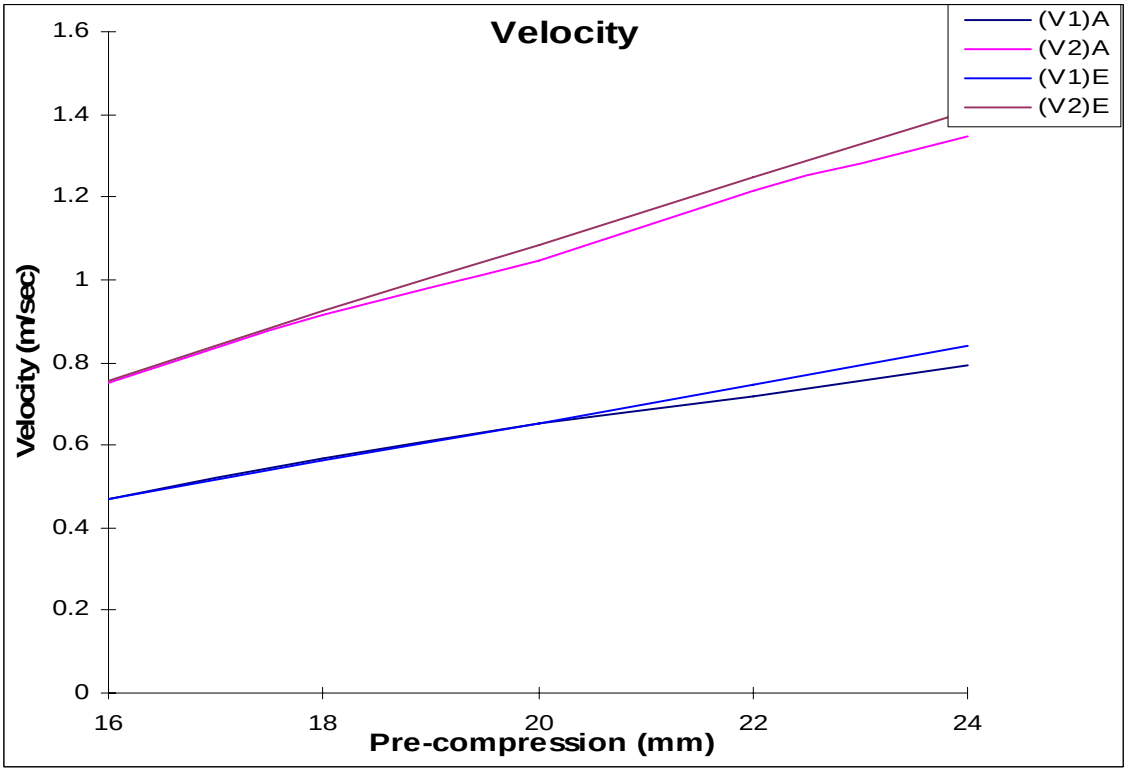

Fig 6.7: Comparison of Body Velocity from ADAMS and Experiment

From Fig 6.6, it is clear that experimental and ADAMS energy loss matches up to *20mm* pre-compression after it diverges slightly. This is because ADAMS guide friction model is same as that of experimental model only up to that range and after that it changes its properties. Energy loss in friction is much higher as compared to energy loss in impact and increasing rapidly with the pre-compression. Also, energy loss at take-off is larger than at touch-down. This is also increasing with pre-compression because velocity at take-off is larger than at touch-down.

Fig 6.7 shows comparison of ADAMS velocity with experimental velocity at touch-down and take-off point. For experimental readings, velocity of body is linearly increases with pre-compression. But for ADAMS, it reduces after pre-compression becomes *18mm.*

Chapter 7

CONCLUSIONS AND FUTURE WORK

7.1 Conclusions:

The energy pumping mechanism is successfully tested on a hopper for effectiveness and range of energy. A low weight vertical hopper is designed and tested by considering hopper design feature at design stage. Low weight of leg with respect to body reduces energy loss at touch-down and take-off. From this work we can conclude,

1. Hopper is tested for five different pre-compression starting from *16mm* to *24 mm* and hopping frequency of *5Hz*. As below *16mm* pre-compression, actuator doesn't get enough time to pump the energy and to release it fully. Because of that hopper stops within 5-7 hops.
2. From experimental results, energy loss in guide friction is much higher than energy loss in impact. But the actual hopper model doesn't have any guide so this energy will be utilized for increase in height of body.
3. From this experimentation, we can predict maximum friction loss on real hopper because it will be lesser than (E_{f2}+E_{f3}).
4. Comparison of hopper energy loss from ADAMS simulation package and experiment analysis shows friction properties of LM guide on equivalent sliding joint.

.

7.2 Future Works:

1. This hopper model can be studied for transient hopping.
2. The high speed video-graphic camera is used to observe the velocity at touch-down and take-off.
3. The ratchet of this hopper is replaced by one which has smaller pitch to study for fine hopping parameters.
4. Implementing off-set mass, this hopper can be studied as planer hopper by guiding it linearly or developing suitable control algorithms used by Gebretsadik [10].
5. The new hopper can be designed for tensile spring with the same latching mechanism. Because presence of guide in compression spring leads frictional energy loss.

REFERENCES

1. Raibert Marc H., “Legged Robots that Balance”, MIT Press, Cambridge MA, 1986.
2. Raibert Marc H., “Running with Symmetry”, The International Journal of Robotics Research, Vol. 5, No.4, Winter 1986, pp45-61
3. Raibert, Marc H. and Brown, H.B., Jr, ”Experiments In Balance With a 2D One-Legged hopping Machine,” Journal of Dynamics Systems, Measurement ,and Control, Vol.106, March 1984, pp75-81
4. Akihiro Sato, “A Planner Hopping Robot with One Actuator”, M.E. Thesis, McGill University, Montreal, Caneda, 2004.
5. A. Sato and M. Buehler, “A Planar Hopping Robot with One Actuator: Design, Simulation, and Experimental Results,” IEEE/RSJ 17th International Conference on Intelligent Robots and Systems (IROS), pp. 3540-3545, 2004
6. Zeglin, G., “The Bow Leg Hopping Robot,” PhD Thesis, Carnegie Mellon University, Pittsburgh, Pennsylvania, 1999.
7. T. Akinfiev, M. Armada, and H. Montes, “Vertical Movement of Resonance Hopping Robot with Electric Drive and Simple Control System”, Proc. of IEEE International conference on control and automation, ICRA ’04, New Orleans, USA, vol. 4,Pp. 4220-4245, Apr/May2004.
8. Shanmugnathan, P.V., “Dynamics & Stabilization of Under-Actuated Monopedal Hopping,” PhD Thesis, Indian Institute of Technology, Bombay, 2003.
9. S. Sharma, Dahrmendra, “Springy Leg Design for Hopping Robot,” M. Tech Thesis, Indian Institute of Technology, Bombay, 2004.
10. Hailu Gebretsadik, “Dynamic Analysis and Design of a Single Legged, Energy Efficient, Hopping Robot”, M. Tech Thesis, Indian Institute of Technology, Bombay, 2005.
11. Hamidreza Dokt Tagirad, “Analysis, Design, and Control of Hopping Robot”, M.E.Thesis, McGill University, Montreal, Canada, 1993.
12. J. E. Shigley and C. R. Mischke. Mechanical Engineering Design. McGraw Hill Company Inc., New York

13. V. B. Bhandari, Design of Machine Elements. Tata McGraw Hill Publishing Company, New Delhi
14. F. Roos, H. Johansson, Jan Wikander, "Optimal Selection of motor and gear head in mechatronic applications" Mechatronics, Volume 16, Issue 1, Pages 63-72 *(*February 2006*)*
15. http://www.faulhaber-group.com/uploadpk/e_2642CR_DFF.pdf as seen on date 6th July 2007.
16. http://www.faulhaber-group.com/uploadpk/e_HEDS_HEDM_DFF.pdf as seen on date 6th July 2007.
17. http://www.faulhaber-group.com/uploadpk/e_261_MIN.pdf as seen on date 6th July 2007.

APPENDIX

APPENDIX A

A.1 Flight and Stance time:

The hopper falls from altitude and first touched the ground after CM of body gets displaced by Δh. The ideal hopper (without any constraints) flight time (t_f) is given by;

$$\Delta h = 0.5g(t_f/2)^2 \rightarrow \therefore t_f = \sqrt{8\Delta h/g}\ Sec \ldots\ldots\ldots\ldots\ldots\ldots\ldots\ldots\ldots\ldots\ldots\ldots A.1$$

Hopper velocity at touch-down is given by:

$$V_1 = \sqrt{2g\Delta h} \ldots\ldots\ldots\ldots\ldots\ldots\ldots\ldots\ldots\ldots\ldots\ldots\ldots\ldots\ldots\ldots\ldots\ldots\ldots\ldots A.2$$

The momentum at impact is exactly reversed by the constant force of spring applied over the stance period:

$$M\Delta V = F_0 t_s = -2MV_1 \ldots\ldots\ldots\ldots\ldots\ldots\ldots\ldots\ldots\ldots\ldots\ldots\ldots\ldots\ldots\ldots\ldots\ldots\ldots\ldots A.3$$

Solving for stance time;

$$t_s = \frac{M}{F_0}\sqrt{8g\Delta h} \ldots\ldots\ldots\ldots\ldots\ldots\ldots\ldots\ldots\ldots\ldots\ldots\ldots\ldots\ldots\ldots\ldots\ldots\ldots\ldots A.4$$

Total hopping cycle time is; $t_t = t_s + t_f$

APPENDIX B

B.1 DC motor and Gear-head:

DC motors are often applied where they momentarily deliver three or more times their rated torque. In emergency situations, dc motors can supply over five times rated torque without stalling (power supply permitting). Dc motors feature a speed, which can be controlled smoothly down to zero, immediately followed by acceleration in the opposite direction -- without power circuit switching. And dc motors respond quickly to changes in control signals due to the dc motor's high ratio of torque to inertia.

B.2 Micro-Motor

DC micro-motors offer good efficiencies and a high peak load through use of premium ferrite materials and optimized magnet systems. The DC micro-motor comes in 2 different versions each with graphite commutation which ensures long-life even under overload conditions.

DC micro-motors features

- Extremely low moment of rotor inertia
- High precision performance
- Low brush contact resistance
- Less power required
- Graphite commutation achieves extended service life

Coreless DC micro motor

- Coreless rotor means no cogging or preferred rotor position
- No iron losses
- Extremely low current consumption
- Low starting voltage
- Low rotor inertia for extremely fast acceleration and braking
- Extremely light and compact
- Smooth and accurate speed, position, and torque control
- Custom systems available from design to production

- Higher power to volume than other DC motor technologies
- High precision gearboxes available in all sizes
- Feedback components available in all sizes
- Control electronics available for all motor series

B.3 DC Micro-Motor Specifications:

Nominal voltage (U_n)	24V
Output power (P_2max)	23.2W
Efficiency (η_{max})	79%
No-load speed	6400 rpm
No-load current (with shaft ø 4.0 mm)	0.058A
Stall torque (M_H)	139mNm
Speed constant (K_n)	276 rpm/Volt
Torque constant (K_M)	34.6 mNm/A
Current constant (K_I)	0.0029A/mNm
Slope of n-M curve ($\Delta n / \Delta M$)	46.0rpm/mNm
Mechanical time constant (τ_m)	5.4ms
Rotor inertia (J)	11gcm^2
Angular acceleration (α_{max})	120x10^{3}rad/s^2
Shaft load max.:	
– With shaft diameter	4
– Axial at 3 000 rpm	2N
– Axial at standstill	20N
Weight	114 grams

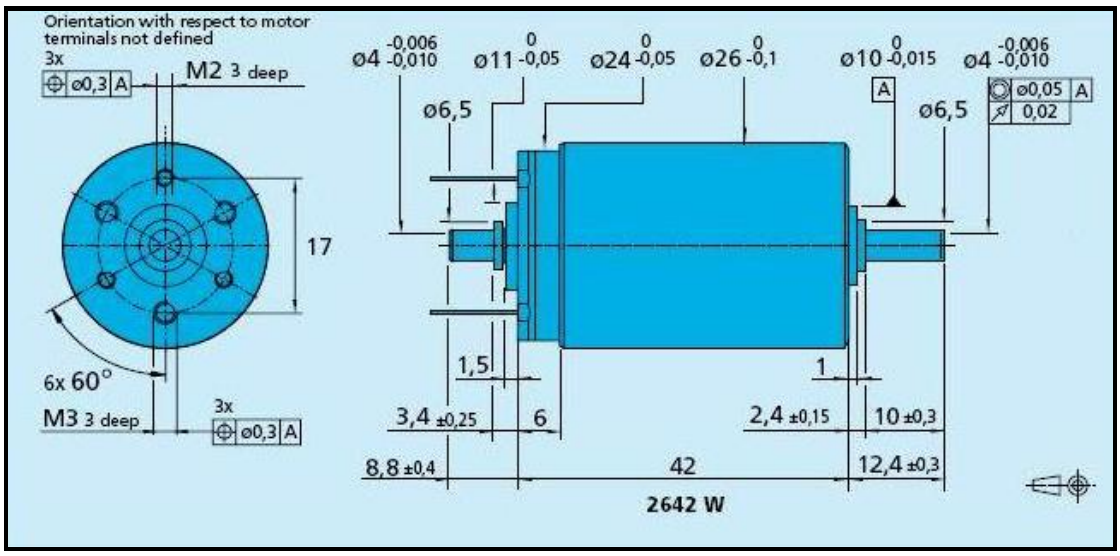

Fig B1: CAD drawing of DC motor

B.4 Planetary Gear head:

Reduction Ratio	3.71:1
Housing material	Inox steel
Gearing material	steel
Recommended maximum input speed recommended for continuous operation	4000rpm
Weight without motor	93 gram
Efficiency	88%
Output torque for continuous operation	1.1 Nm
Shaft load maximum	
Radial load (10mm from face)	≤150N
Axial load	≤100N

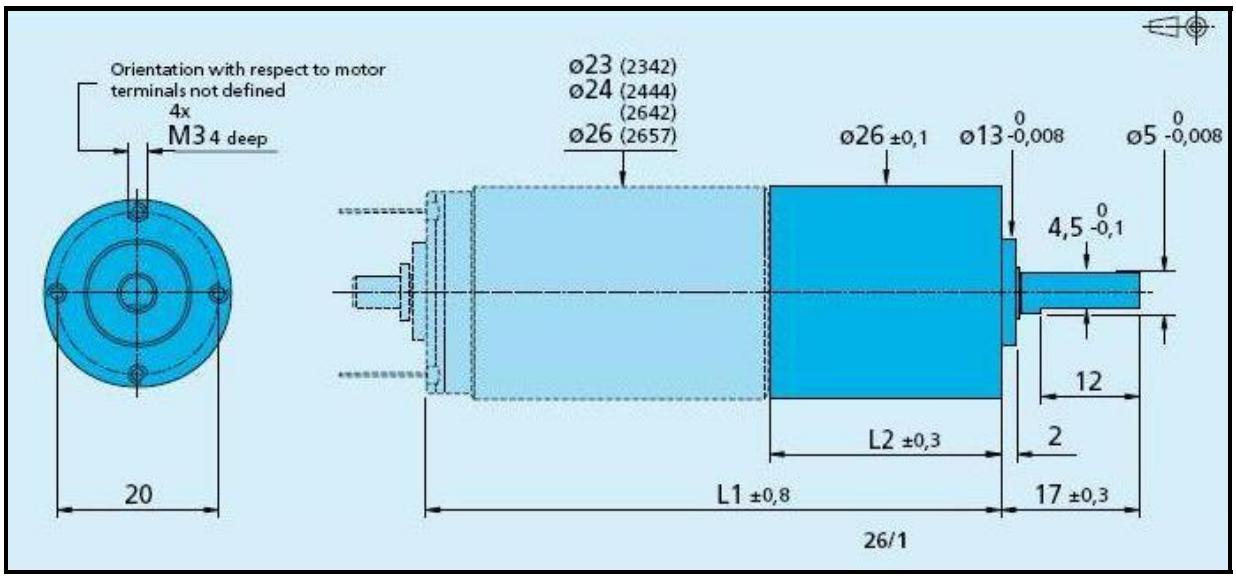

Fig B2: CAD model of motor with gear-head

T_{RMS} Calculations:

$$T_{RMS} = \sqrt{\frac{1}{T}\int_0^T (T_{inst})^2}$$

$$\therefore T_{RMS} = \sqrt{\frac{1}{0.1}\int_0^{0.1} (r \times k \times x)^2 \, dt}$$

$$\therefore T_{RMS} = \sqrt{\frac{1}{0.1}\int_0^{0.1} \{2.5 \times 2 \times 0.015(1-\cos\omega t)\}^2 \, dt} \rightarrow \omega = \frac{\pi}{0.1}$$

$$\therefore T_{RMS} = 0.075 \times \sqrt{\frac{1}{0.1}\int_0^{0.1} (1 - 2\cos\omega t + \cos^2 \omega t) dt}$$

$$\therefore T_{RMS} = 0.23717 \times \sqrt{\int_0^{0.1} (1 - 2\cos\omega t + 0.5(\cos 2\omega t + 1) dt}$$

$$\therefore T_{RMS} = 0.09185 Nm$$

$$\therefore T_m = 0.09185 / 3.71 = 0.02475 Nm$$

APPENDIX C

C.1 Optical Encoder:

Specifications

Lines per revolution	500
Signal output, square wave	2+1 index
Current consumption, typical (V_{CC} = 5 V DC)	57mA

The following figure shows optical encoder details and connector.

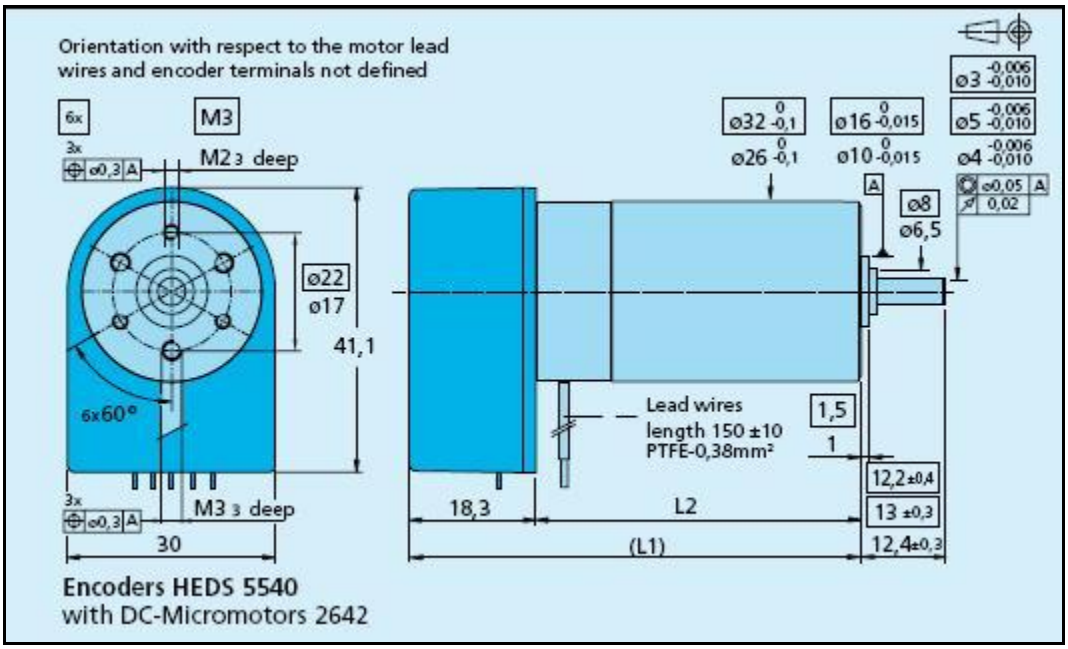

Fig C.1: Encoder details

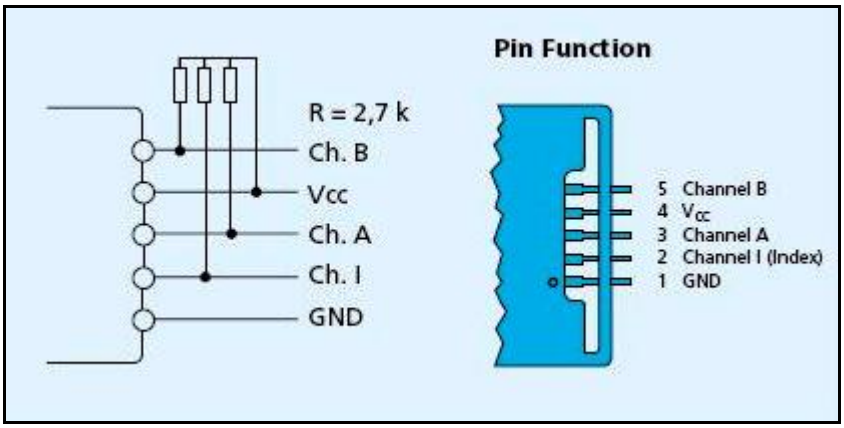

Fig C.2 Encoder Connector

C.2 dSPACE Controller Board:

The DS1104 R&D Controller Board upgrades your PC to a development system for rapid control prototyping (RCP). The real-time hardware – based on the PowerPC 603e microprocessor – and its I/O interfaces make the board ideally suited for developing controllers in various fields – in both industry and university.

The following illustration gives an overview of the architecture and the functional units of the DS1104:

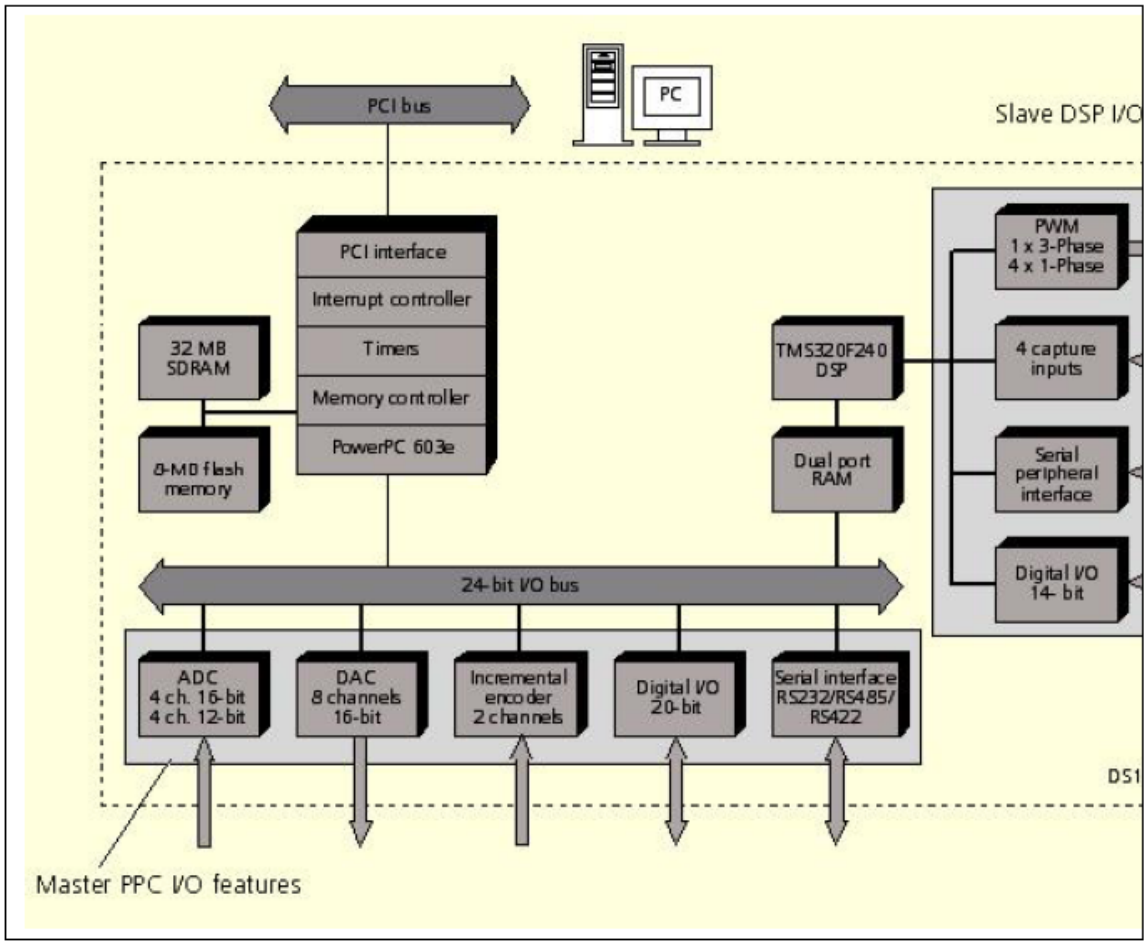

Fig C3: DS1104 controller Board Layout and features

The Following table shows dSPACE specifications

Table C.1: The data sheet of the DS1104 (specifications) R&D Controller Board.

Parameter	**Characteristics**
Processor	• MPC8240 processor with PPC603e core and on-chip peripherals • 64-bit floating-point processor • 250 MHz CPU • 2 x 16 KB cache; on-chip • On-chip PCI bridge (33 MHz)
Memory	• Global memory: 32 MB SDRAM • Flash memory: 8 MB
Host interface	• 32-bit PCI host interface 33 MHz ±5 % • 5 V PCI slot
Timer	• 1 sample rate timer (decrementer): 32-bit down counter, reload by software, 40 ns resolution • 4 general purpose timer: 32-bit down counter, reload by hardware, 80 ns resolution • 1 time base counter: 64-bit up counter, 40 ns resolution, range 23400yrs
Interrupt controller	• 5 timer interrupts • 2 incremental encoder index line interrupts • 1 UART interrupt • 1 slave DSP interrupt • 1 slave DSP PWM interrupt • 5 ADC end of conversion interrupts • 1 host interrupt • 4 user interrupts from the I/O connector

ADC 1 x 16-bit ADC with mux	• 4 muxed channels equipped with one 16-bit sample & hold ADC Note:5ADC channels (1x16-bit+4x12-bit) can be sampled simultaneous • 16-bit resolution • ±10 V input voltage range • 2 ms conversion time • ±5 mV offset error • ±0.25 % gain error • 4 ppm/K offset drift • 25 ppm/K gain drift • >80 dB signal-to-noise ratio (SNR)
ADC 4 x 12-bit ADC	• 4 channels each equipped with one 12-bit sample & hold ADC Note: 5 ADC channels (1 x 16-bit + 4 x 12-bit) can be sampled simultaneous • 12-bit resolution • ±10 V input voltage range • 800 ns conversion time • ±5 mV offset error • ±0.5 % gain error • 4 ppm/K offset drift • 25 ppm/K gain drift • >65 dB signal-to-noise ratio (SNR)
Digital I/O	• 20-bit parallel I/O • Single bit selectable for input or output • ±5 mA maximum output current • TTL output/input levels

DACs 8 x 16-bit DAC	• 16-bit resolution • ±10 V output voltage range • ±5 mA maximum output current • Max. 10 ms settling time (full scale, accuracy 1/2 LSB) • ±1 mV offset error • ±0.1 % gain error • >80 dB signal-to-noise ratio (SNR)
Digital Incremental Encoder Interface (2 x 24 bit)	• 2 channels • Selectable single-ended (TTL) or differential (RS422) input • Fourfold line subdivision • Max. 1.65 MHz input frequency, i.e. fourfold pulse counts up to 6.6 MHz • 24-bit loadable position counter • Reset on index • 5 V/0.5 A sensor supply voltage
Serial interface	• 1 serial UART • Selectable transceiver mode: RS232/RS422/RS485 • Max. baudrate RS232: 115.2 kBaud • Max. baudrate RS422/RS485: 1 MBaud
Physical size	PCI 185 x 106.68 mm (7.28 x 4.2 in)
Ambient temperature	0 ... 55 ºC (32 ... 131 ºF)
Cooling	Active cooling by fan

Slave DSP subsystem	• Texas Instruments TMS320F240 DSP • 16-bit fixed-point processor • 20 MHz clock frequency • 64 K x 16 external program memory • 28 K x 16 external data memory • 4 K x 16 dual-port memory for communication • 16 K x 16 flash memory • 1 x 3-phase PWM output • 4 x 1-phase PWM output • 4 capture inputs • SPI (serial peripheral interface) • Max. 14-bit digital I/O • TTL output/input levels for all digital I/O pins • ±13 mA maximum output current
Power supply	• +5 V ±5 %, 2.5 A • +12 V ±5 %, 0.3 A • –12 V ±5 %, 0.2 A
Power consumption	18.5 W

ACKNOWLEDGEMENT

I would like to express my sincere thanks and gratitude to my guide Prof. B. Seth for enduring support and precious guidance given throughout the course of my work. I would not have reached this current level of completeness without his help. A thank goes to all my colleagues at IIT Bombay for the unflinching help they have offered when ever needed.

Date: July 12, 2007 Vitthal N. Londhe

Place: Mumbai (05310006)